Bioorganic Chemistry 111 (2021) 104877

Contents lists available at ScienceDirect

Bioorganic Chemistry

journal homepage: www.elsevier.com/locate/bioorg

Synthesis of new substituted pyridine derivatives as potent anti-liver cancer agents through apoptosis induction: *In vitro*, *in vivo,* and *in silico* integrated approaches

Ahmed T.A. Boraei *, Elsayed H. Eltamany, Ibrahim A.I. Ali, Sara M. Gebriel, Mohamed S. Nafie *

Chemistry Department, Faculty of Science, Suez Canal University, Ismailia 41522, Egypt

ARTICLE INFO

Keywords:
Liver cancer
Pyridines
Apoptosis
RT-PCR
In vivo

ABSTRACT

Liver cancer is the most common type of cancer in many countries. New studies and statistics show rising liver cancer worldwide, so it is essential to seek new agents for this type of cancer. PIM1 has an attractive target in the discovery of cancer medications as it is very much expressed in a variety of malignancies and influences such as tumorigenesis, cell cycle progression, cellular proliferation, apoptosis, and cell migration. Accordingly, a series of pyridones and pyridine-amides were synthesized and tested for anti-liver cancer activity.

In the synthetic strategy 4,6-diaryl-3-cyano-2-pyridones **3a-n** were synthesized using one-pot four component synthetic method. Structural modifications were done on 4,6-diphenyl-3-cayno-2-pyridone **3a** to enhance the activity. Alkylation in the presence of K_2CO_3 afforded the *O*-alkylated products **4**–**6**. The acetoxy hydrazide **7** was synthesized and cyclized into 1,3,4-oxadiazolethione **8** which alkylated on sulfur to give **10**. Azide-coupling method was used to couple the 2-(pyridin-2-yloxy)acetohydrazide **7** to different amines and amino acid esters to furnish the products **12a-e** and **13a-b**. The synthesized derivatives were subjected to cytotoxic screening against HepG2 and THLE-2 cells, Compounds **10, 12e** and **13a** have a remarkable cytotoxic activity with IC_{50} values (10.7–13.9 μM). Compound **7** was found to be more cytotoxic by showing the lowest IC_{50} value of 7.26 compared to 5-FU (IC_{50} = 6.98 μM). It inhibited cell growth by 76.76%. Additionally, it significantly stimulated apoptotic liver cancer cell death with 49.78-fold (22.90% compared to 0.46% for the control) arresting cell cycle Pre-G1 with 35.16% of a cell population, compared to 1.57% for the control. Moreover, it validated the intrinsic apoptosis through upregulation of P53, and other related genes, with inhibition of anti-apoptotic genes through PIM-1 inhibition.

1. Introduction

Liver cancer was found to be the sixth most commonly occurring cancer and the fourth type of cancer leading mortality worldwide. The estimated new cases were 841,000 and 782,000 deaths in 2018 [1,2]. The Provirus Integration in Maloney (PIM) kinases are highly expressed in many kinds of hematological and solid cancers. PIM kinases which are known as (protooncogenes) regulate the network of signaling pathways that are critical for tumorigenesis and growth, making PIM kinases attractive drug targets [3]. PIM-1 has a significant role in the regulation of the cell cycle through phosphorylation of the Cdc25 phosphatases and cell-cycle inhibitors [4,5] also it stimulates the transition of cells from G1 to S phase through the phosphorylation and activation of the phosphatase Cdc25A [6], causing an enhancement of Cdc25A-mediated cellular transformation. Moreover, PIM-1 is also associated with drug resistance and its level of expression which was reported to be upregulated in mitoxantrone- and docetaxel-resistant cancer cell lines [7,8]. PIM kinases have become attractive therapeutic targets for cancer treatment because they are involved in cancer-specific pathways and upregulated in many cancers [9,10]. Since, pyridine motif is found in many biologically and pharmaceutically active agents [11,12] for example, Etoricoxib is non-steroidal anti-inflammatory drug [13], amlodipine, nifedipine, and clevidipine are acting as calcium channel blockers [14].

Moreover, it was found that the pharmacophoric features of some anticancer drugs, such as Veliparib, Niraparib, Rucaparib and Olaparib is strongly dependent on the presence of the amide group either primary or embedded in a heterocyclic ring that serve as hydrogen bond donors

* Corresponding authors.
E-mail addresses: ahmed_tawfeek83@yahoo.com (A.T.A. Boraei), mohamed_nafie@science.suez.edu.eg (M.S. Nafie).

https://doi.org/10.1016/j.bioorg.2021.104877
Received 7 January 2021; Received in revised form 9 March 2021; Accepted 25 March 2021
Available online 29 March 2021

for the interaction with biological targets [15,16]. Additionally, the most potent PIM inhibitor identified to date 6-phenyl-*N*-(pyridin-3-yl) picolinamide (LGB321), its structure contains pyridine, amine, and amide groups which are essential for hydrogen bond interactions with the residues of the ATP-binding site of PIM-1 [17,18] Fig. 1.

As part of our continued efforts for synthesis and discovery of new anticancer hits [19–22], though stepwise biology plan including cytotoxic screening, apoptosis induction [23–25]. This work includes the design and synthesis of several pyridine derivatives and evaluating their activity towards liver cancer. Results disclosed that 2-(3-cyano-4,6-diphenylpyridin-2-yloxy)acetohydrazide has the most potent activity. It significantly impeded cell proliferation and cell migration by interfering with PIM-1 enzymatic activity.

2. Results and discussion

2.1. Chemistry

Four component one-pot synthesis of various substituted 4,6-diaryl-3-cyano-2-pyridones **3a-n** from the reflux of aromatic aldehydes, ketones, ethyl cyanoacetate, and ammonium acetate in *n*-butanol for 1–3 h was performed Scheme 1, Table 1. The NMR of pyridone **3a-n** displayed the pyridone NH around 12.50 ppm, and carbonyl carbon was detected around 162.5 ppm.

Alkylations of 4,6-diphenyl-3-cayno-2-pyridone **3a** with benzyl bromide, phenacyl bromide, and ethyl chloroacetate were done using K_2CO_3 as proton scavenger in acetone and DMF which afforded the *O*-alkylated product **4**–**6** respectively (Scheme 2). The ^{13}C NMR of the alkylated products **4**–**6** showed the methylene carbon at 68.8, 69.3, and 64.2 ppm respectively, which recommends the alkylation at oxygen, not nitrogen.

Construction of a system including both pyridine and 1,3,4-oxadiazole moieties was achieved by synthesizing hydrazide **7** from the hydrazinolysis of the ester **6**. The hydrazide **7** was reacted with carbon disulfide in ethanol containing aq. KOH to afford the dithioic acid **8** on stirring and the desired the pyridinyl-oxadiazolthione **9** upon reflux. pyridinyl-oxadiazolthione **9** was alkylated with phenacyl bromide in the presence of K_2CO_3 to give the *S*-alkylated product **10** (Scheme 3). The ^1H NMR of the hydrazide **7** revealed the NH_2 protons at 4.30 ppm and the NH proton at 9.39 ppm. Due to cyclization the ^1H NMR a broad signal at 14.64 ppm for the delocalized NH and ^{13}C NMR displayed a new signal at 178.7 ppm for the thiocarbonyl group. The ^{13}C NMR of the phenacylated product **10** displayed a new methylene carbon signal at 39.7 ppm which suggests the alkylation at sulfur, not nitrogen.

Coupling of the pyridine-hydrazide scaffold **7** with various amines and amino acid methyl esters was done through azide-coupling strategy in which the hydrazide **7** was converted into azide **11**. The latter was allowed to react with different amines like propyl amine, benzyl amine, tetradodecyl amine, allyl amine and piperidine to give the amides **12a-e** respectively, and with glycine methyl ester HCl and L-leucine methyl ester HCl in the presence of Et_3N to give the coupled products **13a-b** (Scheme 4). The amines and amino acid NMR showed the characteristic signals. Compounds **13a-b** NMR revealed the methoxy protons at 3.60 ppm and the respective methoxy carbons at 65.0 ppm.

2.2. Biology

2.2.1. Cytotoxicity using the MTT assay

To estimate their selectivity, selected compounds were screened for their cytotoxic activity against the liver cancer cell lines (HepG2), and the normal liver cells. As shown in Table 2, and Fig. 2, which summarizes the IC_{50} values of all tested derivatives. Among them, compound **7**

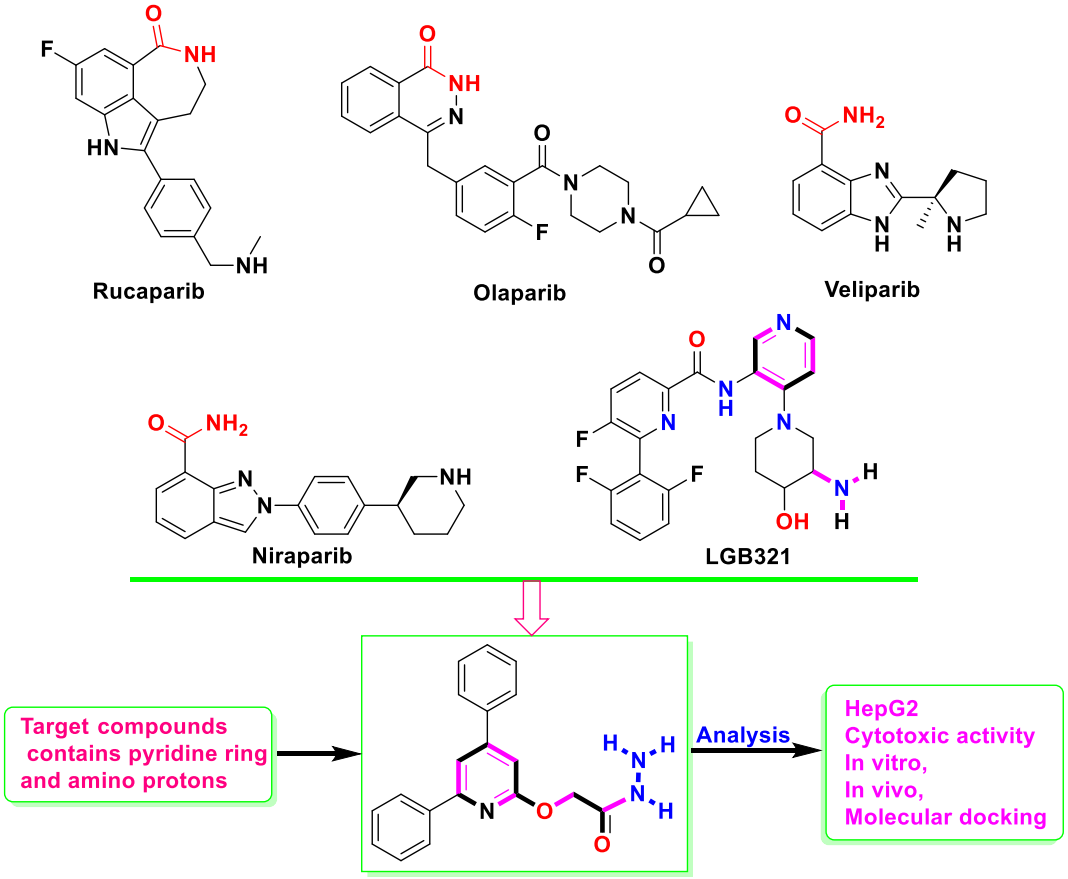

Fig. 1. Structures of selected FDA-approved anticancer drugs showing the significance of pharmacophoric amide group in designing the target PIM-1inhibitors.

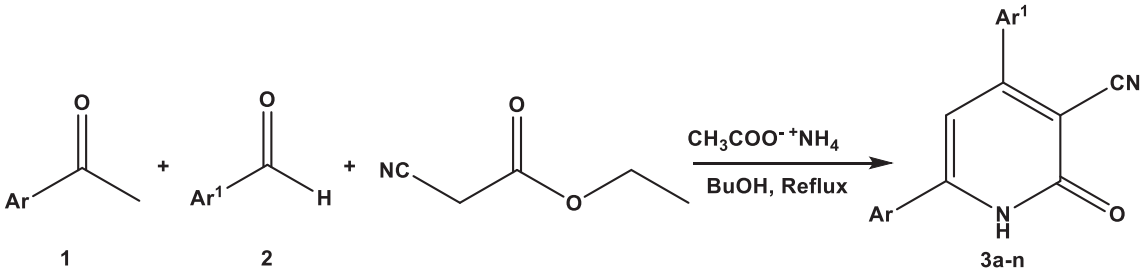

Scheme 1. Four component one-pot synthesis of 2-pyridinones **3a-n.**

Table 1
The aromatic ketones and aldehydes used for the synthesis of 2-pyridinones **3a-n.**

m.p	Ar^1	Ar	Entry
313	C_6H_5-	C_6H_5-	**3a**
313–315	C_6H_5-	3-NH_2-C_6H_4-	**3b**
312	C_6H_5-	4-NH_2-C_6H_4-	**3c**
294–296	C_6H_5-	4-Br-C_6H_4-	**3d**
260–262	C_6H_5-	4-OCH_3-C_6H_4-	**3e**
271–273	C_6H_5-	Cyclohexel	**3f**
312	4-OCH_3-C_6H_4-	C_6H_5-	**3 g**
302	4-NO_2-C_6H_4-	C_6H_5-	**3 h**
240	3-OCH_3-C_6H_4-	C_6H_5-	**3i**
310–312	4-$N(CH_3)_2$-C_6H_4-	C_6H_5-	**3j**
300	2-furyl	C_6H_5-	**3 k**
304	3-Cl-C_6H_4	4-Cl-C_6H_4-	**3 l**
275–277	4-OCH_3-C_6H_4	4-Cl-C_6H_4-	**3 *m***
300–302	4-OCH_3-C_6H_4	3-NH_2-C_6H_4-	**3*n***

was found to be more cytotoxic by showing the lowest IC_{50} value of 7.26 μM compared to 5-FU (IC_{50} = 6.98 μM). It inhibited the cell growth by 76.76%. Compounds **10, 12e, and 13a** have remarkable cytotoxic activity with IC_{50} values (10.7–13.9 μM). Additionally, most of the tested derivatives were safe (non-toxic) against the normal liver cells. The results recommended hit **7** for further studies.

2.2.2. *Apoptotic investigation*

2.2.2.1. Annexin V/PI with cell cycle analysis. For the investigation, the apoptosis-inducing activity of compound compounds **7** (IC_{50} = 7.26 μM) in HepG2, cells after treatment were subjected to flow cytometric analysis of Annexin V/PI staining with cell cycle analysis to determine the cell population in different cell cycle phases. As seen in Fig. 3 (upper panel), compound **7** significantly stimulated apoptotic liver cancer cell death with 49.78-fold; it increased apoptosis ratio by 22.90% (2.67% for early and 20.23% for late apoptosis) compared to 0.46% (0.39% for early and 0.07% for late apoptosis) for the control. Hit compound **7** treatment induced the apoptotic cell death more than the necrotic one, it stimulated necrotic cell death with 11.04-fold (12.26%, compared to 1.11% for the control). Moreover, treated HepG2 cells with compound **7** was subjected to DNA flow cytometry to determine at which cell cycle, the cell proliferation was arrested. As seen in Fig. 3 (lower panel). The compound treatment indignantly increased Pre-G1 with 35.16% population, compared to 1.57% for the control. While cell population at other cell phases are not significantly changed. Our results agreed with Bachmann et al. [26] who reported that the PIM-1 inhibition would have apoptosis-inducing activity through cell cycle arrest.

2.2.2.2. RT-PCR. HepG2 cells were treated with compound **7** (IC_{50} = 7.26 μM for 72 h), following the routine work of RT-PCR test to investigate its apoptotic pathway. The apoptotic pathway was investigated by following the mRNA expression of P53, BAX, PUMA, Caspases 3, 8 9 as pro-apoptotic, Bcl-2 as antiapoptotic gene, and the PIM-1 kinase genes.

As shown in Fig. 4, compound **7** significantly activated the level of P53 gene (≈5.74-fold) and PUMA and BAX levels with ≈6.09-fold and 7.12-fold, respectively. The compound increased the mRNA levels of casp-3 (4.64-fold), casp-8 (9.09-fold), casp-9 gene (6.27-fold), while it significantly inhibited the anti-apoptotic Bcl-2 gene with 0.41-fold, and the PIM-1 kinase gene expression with 0.45-fold. Thus, up-regulation of, P53, Bax, PUMA, Caspases-3, -8, -9 and downregulation of BCL2, PIM-1 kinase genes were induced by compound **7** relative to control, propose induction of intrinsic and extrinsic apoptosis pathway in the treated liver cancer cell line, The results are following the decreased levels of PIM-1 kinase activates apoptosis pro-apoptotic proteins as previously reported in [27], and inhibits the antiapoptotic genes as reported in 2020 [22].

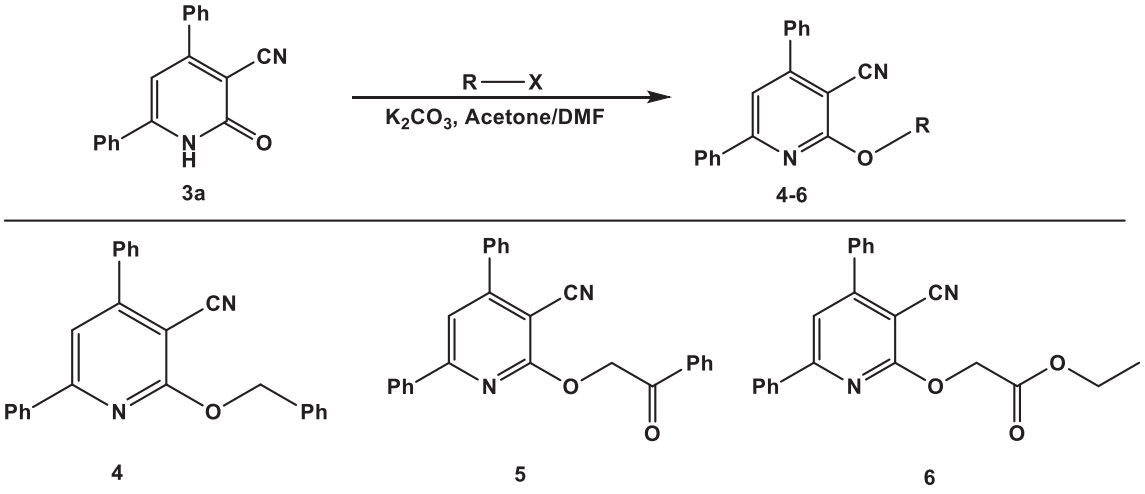

Scheme 2. Alkylation of 4,6-diphenyl-3-cyano-2-pyridones **3a** with benzyl bromide, phenacyl bromide, and ethyl chloroacetate.

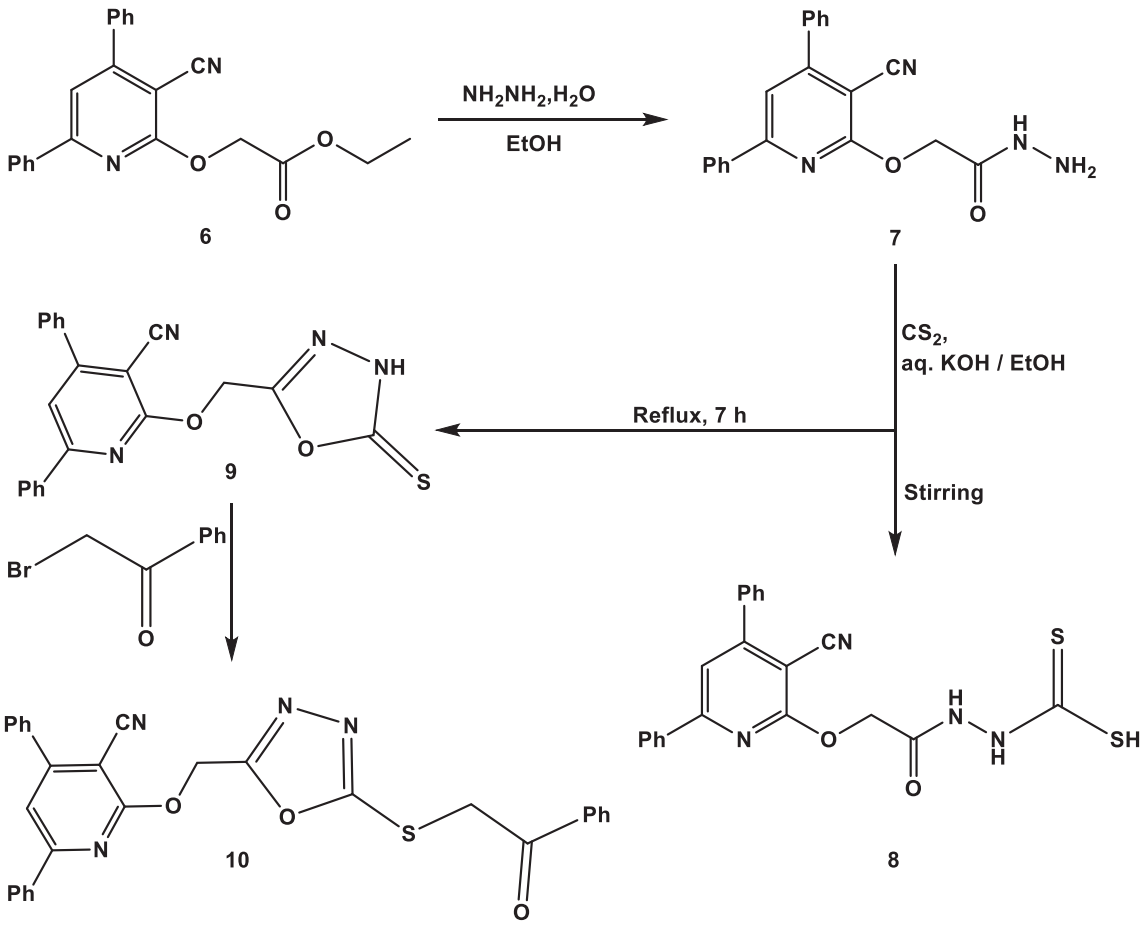

Scheme 3. Hydrazinolysis of the ester **6** and heterocyclization of the respective hydrazide **7.**

2.2.3. *In vivo*

2.2.3.1. Antitumor potentiality. After ten days of tumor cell inoculation, masses of solid Ehrlich carcinoma (*SEC*) began to appear. Mice were treated with compound **7** at its LD_{50} dose (5 mg/kg BW, IP) for evaluation of its *in vivo* activity against *SEC* development. A total of seven doses of the compound started on day 7 after tumor inoculation. At the end of the procedure, weight and volume of the solid tumor masses were measured. During the experimental duration, an increase in solid tumor weight of around 130 mg was observed via tumor development. The antitumor effect of compound **7** and 5-FU was elucidated; there was a significant decrease in the solid tumor mass by 47.92% (67.87 mg) and 62.68% (48.63 mg), respectively compared to control (130.32 mg) Fig. 5. Accordingly, treatments of compound **7**significantly inhibited the percentage of tumor inhibition by 36.05% in tumor volume (32.1 mm^3) relative to 5-FU treatment with tumor inhibition ratio 64.14% (18 mm^3), compared to control (50.2 mm^3). One of the valuable results, is worthy to be mentioned that in **7**-treated-*SEC* group, one or two mice had not formed remarkable tumor mass compared to the *SEC* control group in which, mice were found to move very difficult due to the large tumor mass in their legs.

2.2.3.2. Hematological and biochemical investigations. At the end of the experiment, animals from different groups were sacrificed, and blood samples were collected for hematological parameters including Hb, RBC's and WBC's levels, and serum for determination of liver enzymes ALT, AST levels, and kidney parameters urea and creatinine levels. As summarized in Table 3, in *SEC*-bearing mice. All CBC parameters were changed in the *SEC* control, where Hb content and RBC's were significantly decreased to be 4.02 (g/dL) and 3.01 (10^6/μL), respectively. While WBC's count was significantly increased to be 5.04 (10^3/μL) compared to the normal control levels. Reduced levels of hemoglobin, RBC's and elevation of WBC's counts are routine consequences of tumor propagation [28,29] Upon treatment with compound **7,** CBC levels were nearly retained to their normal values, where it elevated the Hb (6.32 g/dL), RBC's (4.87 10^6/μL) and reduced the WBC's (3.98 10^3/μL) levels. Interestingly our results following that of Gad et al. 2020 [29] study illustrated the ameliorative effect in the hematological parameters after the treatment with the tested compound.

Regarding biochemical parameters, due to hepatocellular damage following tumor inoculation, liver enzymes (ALT and AST) were significantly elevated to be significantly elevated to 74.56, 89.46 (U/L), respectively, as compared to normal mice 45.63 and 48.49, respectively. Treatment with compound **7**, substantially reduced liver enzymes to be 57.41, 51.11 U/L, respectively indicating a remarkable enhancement in the hepatocellular toxicity induced by *SEC* proliferation. Additionally, for kidney parameters, compound **7** treatment retained the deteriorated urea and creatinine levels to be 28.01 and 0.74 (mg/dL) nearly as normal control 27.32 and 0.83, respectively.

2.2.3.3. Histopathological examinations. These findings were supported by the hepatic histopathological examinations as shown in Fig. 6. In which the compound **7** treatment enhanced their architectures near-normal than in positive control cancer group.

Taken together, treatment of *SEC* mice compound **7** was found to improve in the results of antitumor results of tumor weight and volumes, hematological, biochemical parameters, and histopathological examinations.

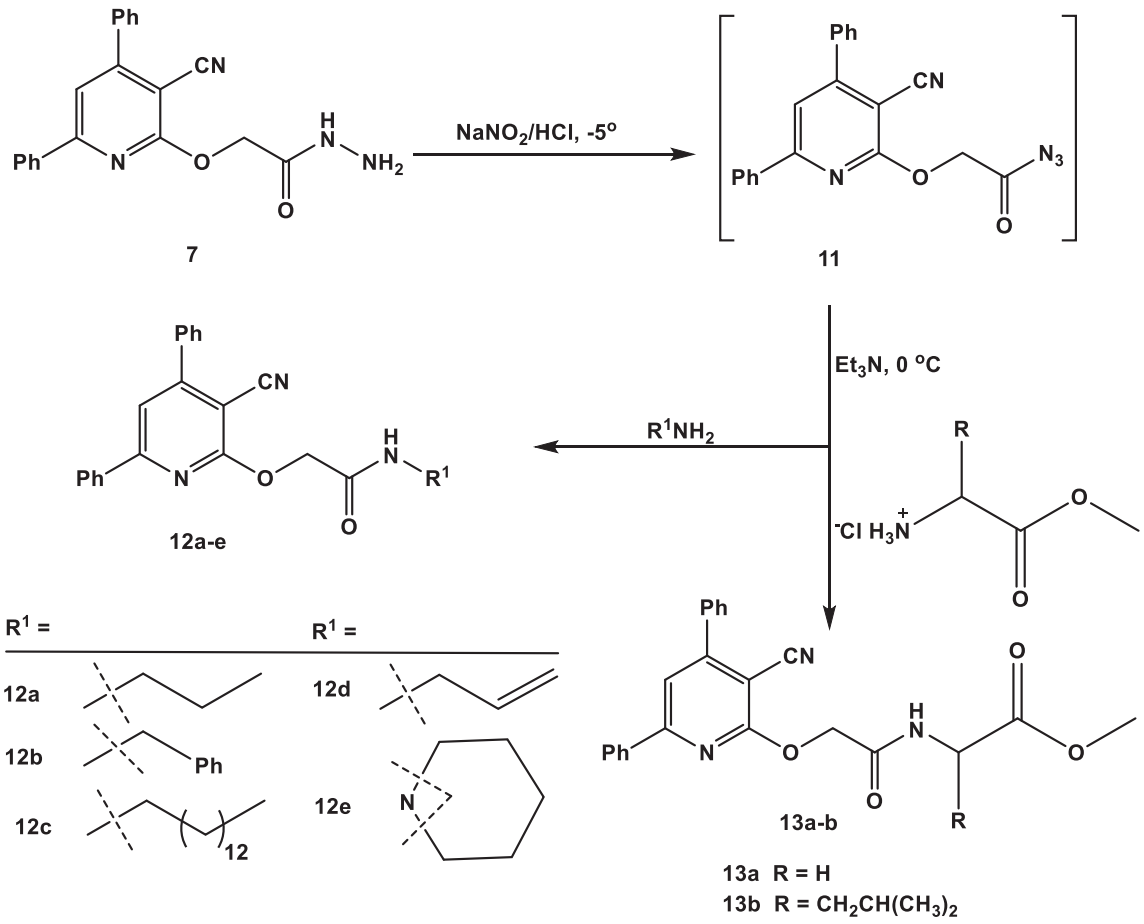

Scheme 4. Azide Coupling of **7** with amines and amino acid esters HCl.

Table 2
Cytotoxic activity of tested derivatives with serial concentrations against HepG2 (liver cancer cell line), and THLE2 (normal liver cells) using the MTT assay.

Compounds	Working concentrations	% of inhibition at 100 μM	IC_{50} ± SD (μM)* HepG2	THLE2
3b	0.01, 0.1, 1, 10, 100 μM	27.52	ND	≥50
3d		36.48	≥50	ND
3e		39.53	≥50	46.7 ± 1.76
3 l		43.21	43.7 ± 1.23	48.2 ± 0.98
3*n*		71.43	19.2 ± 1.01	44.11 ± 0.89
5		41.72	ND	≥50
6		45.56	ND	≥50
7		**76.76**	**7.26 ± 0.34**	**≥50**
8		34.2.3	ND	39.88 ± 0.59
9		62.76	17.6 ± 0.97	≥50
10		74.96	13.4 ± 0.76	≥50
12e		68.83	12.4 ± 0.83	≥50
13a		69.53	13.9 ± 0.98	ND
5-FU		84.72	6.98	ND

* "Values are expressed as Mean ± SD of triplet trials, **ND** is non-determined, and calculated using GraphPad Prism **7** software using nonlinear regression Dose-Inhibition curve fit".

2.2.4. *In silico*

2.2.4.1. Molecular docking. For elucidation, the virtual mechanism of binding, a molecular docking study was carried out to investigate the binding interactions towards PIM-1 kinase 4K0Y and 2OBJ proteins. The co-crystallized ligands of the studied proteins form hydrogen bonds with Lys 67 as the key interactive amino acid. All biologically tested compounds were screened for the molecular docking simulation inside both proteins and most of all exhibited good binding affinities towards both PIM-1 kinases by good interaction mode with the interactive key amino acids and with high binding energies (Full results are supported as supplementary).

Among which, as seen in Table 4, compound **7** was docked inside the protein active site of the two studied proteins and formed one hydrogen bond as HBA with bond lengths 2.39 and 2.03 Å, through its cyano group moiety with the key amino acid Lys 67 like the co-crystallized ligand with binding energy −20.86 and −20.70 Kcal/mol, respectively. Additionally, compound **7** formed arene-cation interaction with Lys 67 inside the 2OBJ protein, and it forms good lipophilic interactions with the nonpolar amino acids Leu 44, Ala 65, Val 52, Ile 185, Ile 104, Leu 120, Leu 174, and Phe 49 inside both receptor pockets. Docking results indicated that the designed compound **7** showed promising binding activity as PIM-1 inhibitors, and this may be the proposed mode of action for anti-liver cancer activity.

2.2.4.2. ADME pharmacokinetics. Compounds with the highest cytotoxic activity against HepG2 cells were subjected to bioinformatics study to predict the physicochemical properties and drug-likeness scores. The candidate drugs that are in line with Lipinski's "five rule" (Ro5) are seen as promising for the future [30–32]. Topological polar area of the

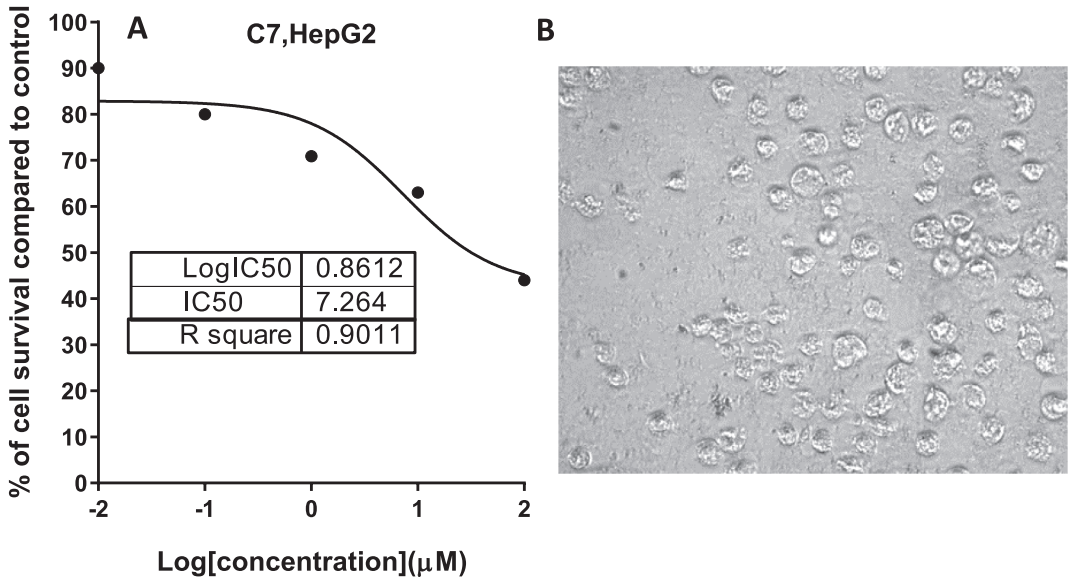

Fig. 2. A. Sigmoidal dose-inhibition curve fit of the percentage of cell survival vs log [conc.] for IC_{50} calculation of compound **7** using GraphPad prism, and **B:** Cytotoxic activity of compound **7** against HepG2 cells.

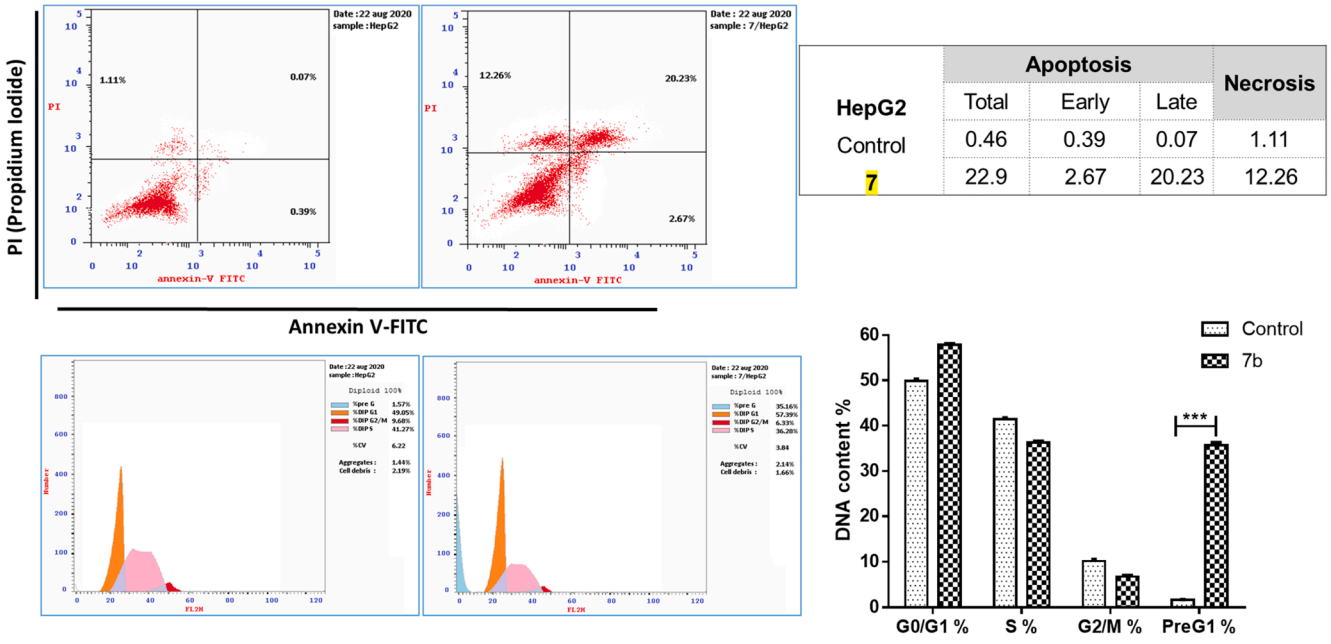

HepG2	Apoptosis			Necrosis
	Total	Early	Late	
Control	0.46	0.39	0.07	1.11
7	22.9	2.67	20.23	12.26

Fig. 3. "FITC/Annexin-V-FITC/PI differential apoptosis/necrosis" (Upper panel) and DNA content-flow cytometry aided cell cycle analyses with bar chart representation (Lower panel) of both untreated and treated HepG2 treated with **7** (IC_{50} = 7.26 μM, 48 h).

surface TPSA values for drug absorption through intestine should be as low as 140, and the blood–brain barrier should be reached as low as 90 $Å^2$ [33,34] The tested compounds were all well-permeable and absorbed as shown in Fig. 7. As seen in Table 5, compounds had 1–4 HB donor and 5–6 acceptors for HB acceptor. Besides, all compounds tested were well tolerated by cell membranes (log P is between 1.18 and 3.38). Veber et al revealed that the rotabile bond number (nrotb) should be ≤10 for controlling conformational changes and for good oral bioavailability [30,35]. All the tested compounds had 1–9 nrotb. Regarding drug-likeness scores, compounds that showed positive values should be considered as drug-like molecules. All the investigated compounds displayed positive values of 0.06–0.12, so they could be considered as drug-like (see Fig. 8).

Finally, Molinspiration virtual screening toolkit was used to calculate the drug-likeness score towards GPCR ligand, ion channel modulator, a kinase inhibitor, nuclear receptor ligand, protease inhibitor, enzyme inhibitor. The larger the value of the score is, the higher is also the probability that the molecule will be active, so compounds **7** exhibited a positive value of 0.11 against kinase protein as seen in Table 6.

3. Experimental section

3.1. General

Melting points were determined in open capillaries on a Temp-melt II melting-point apparatus and the values are uncorrected. Thin-layer chromatography (TLC) was carried out on silica gel 60 F_{254} Aluminium plates (E. Merck, layer thickness 0.2 mm). The spots were

P53	PUMA	BAX	BCL-2	PIM-1 kinase	Casp-3	Casp-8	Casp-9
5.74 ± 0.23	6.09 ± 0.13	7.12 ± 0.13	0.41 ± 0.04	0.45 ± 0.04	9.09 ± 0.11	4.64 ± 0.31	6.27 ± 0.42

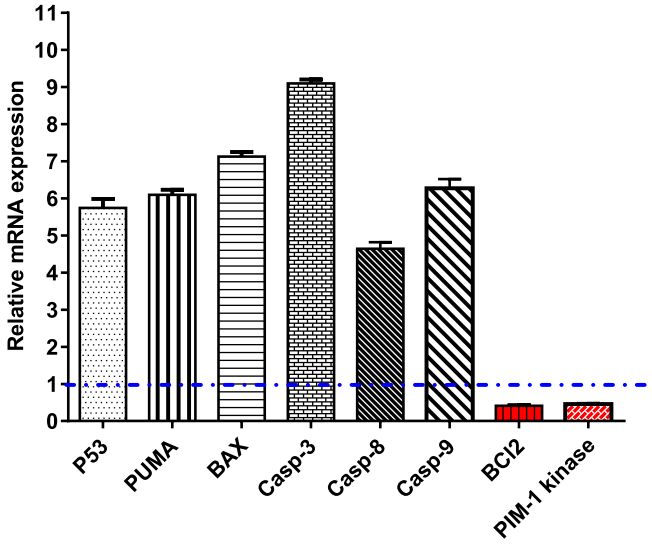

Fig. 4. RT-PCR analysis of the apoptosis-related genes was performed after the HepG2 cells were treated with compound **7** (IC_{50} = 7.26 μM) for 72 h.

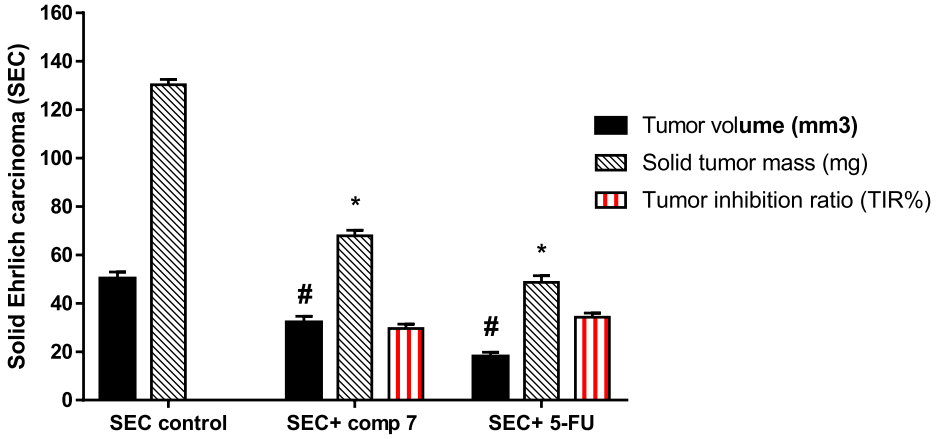

Fig. 5. Antitumor activity of treatment of solid Erlich carcinoma (*SEC*) with compound **7** in mice, compared solid tumor mass, volume, tumor inhibition ratio (TIR %). Values are expressed as Mean ± SEM values of mice in each group (n = 6). Signs of * and # are values with significant differences in tumor volume and tumor weight, respectively compared to *SEC* control using unpaired *t*-test (P ≤ 0.05) using GraphPad prism.

detected by UV lamp. The ^{1}H, ^{13}C NMR spectra were recorded on Bruker 400 MHz-NMR spectrometer operating at 400 and 100 MHz respectively using DMSO-d_6 solvent, at the Microanalytical Laboratory, Sohag University, Egypt. All chemical shifts are reported in ppm values relative to TMS as internal standard. IR spectra were recorded on Fourier Transform Infrared (FT-IR) spectrophotometry (Bruker) a Perking Elmer 1430 ratio recording infrared spectrophotometer using KBR.

3.1.1. Preparation of2-oxo-4,6-diaryl-1,2 dihydropyridine-3-carbonitrile derivatives (3a-n)

A mixture of the selected aromatic aldehyde (0.01 mol.), ketone (0.01 mol.), ethyl cyanoacetate (0.01 mol.), and ammonium acetate (0.08 mol.) was refluxed in *n*-butanol (20.0 mL) for 1–3 h. A precipitate is formed on heating. The mixture is left to cool, filtered, dried, and recrystallized from the appropriate solvent.

3.1.1.1. 2-Oxo-4,6-diphenyl-1,2-dihydropyridine-3-carbonitrile ***(3a)***. Yield: 70% $_{\text{Ethanolas yellowish-brown powder}}$, m.p. 310–311 °C Lit.[1,2] > 300 °C.^{1}H NMR (400 MHz, DMSO-d_6): δ 6.84 (s, 1H), 7.57–7.58 (m, 6H), 7.74 (s, 2H), 7.91 (s, 2H), 12.77 (s, 1H, NH);^{13}C NMR (100 MHz, DMSO-d_6): δ 106.6, 116.9 (CN), 128.2, 128.7, 129.3, 129.4, 130.9, 131.6, 132.8, 136.6, 160.3, 162.5; IR (KBr/cm^{-1}): 1641 (C═O), 2215 (C≡N), 2685 (NH); CHN Calcd. For $C_{18}H_{12}N_2O$ (272.31): C, 79.39; H, 4.44; N, 10.29; Found: C, 79.20; H, 4.53; N, 10.24%.

3.1.1.2. 6-(3-Aminophenyl)-2-oxo-4-phenyl-1,2-dihydropyridine-3-carbonitrile ***(3b)***. Yield: 47 $\%_{\text{acetic acidas yellow powder}}$, m.p. 313–315 °C.$^{1}H$ NMR (400 MHz, DMSO-d_6): δ 5.27 (s, 2H, NH_2), 6.64 (s, 1H), 6.76 (d, *J* = 7.6 Hz, 1H), 7.00 (d, *J* = 9.2 Hz, 2H), 7.15 (t, *J* = 7.6 Hz, 1H), 7.58–7.71 (m, 5H), 12.54 (s, 1H, NH);^{13}C NMR (100 MHz, DMSO-d_6): δ 106.1, 113.0, 115.5, 117.0, 117.1, 128.6, 129.3, 130.0, 130.8, 133.4, 136.7, 149.6, 152.9, 160.2, 162.3; IR (KBr/cm^{-1}): 1599 (C═O), 2218 (C≡N), 2864 (NH), 3355 (NH_2); CHN Calcd. For $C_{18}H_{13}N_3O$ (287.11): C, 75.25; H, 4.56; N, 14.63. Found: C, 75.30; H, 4.53; N, 14.75%.

3.1.1.3. 6-(4-Aminophenyl)-2-oxo-4-phenyl-1,2-dihydropyridine-3-carbonitrile ***(3c)***. Yield: 57%$_{\text{DMF, drops ethanol as yellow powder}}$, m.p. 312 °C.$^{1}H$ NMR (400 MHz, DMSO-d_6): δ 5.93 (s, 2H, NH_2), 6.64 (d, *J* = 7.6 Hz, 3H), 7.55–7.69 (m, 7H), 12.30 (s, 1H, NH);^{13}C NMR (100 MHz, DMSO-d_6): δ 103.7, 113.9, 113.98, 117.5, 118.3, 128.5, 129.2, 129.6, 130.6, 137.0,

Table 3
Hematological and biochemical investigations in the treated groups.

TreatmentsParameter	Normal control	*SEC* control	*SEC* + comp 7(5 mg/kg BW)	*SEC* + 5-FU (5 mg/kg BW)
Hb*# (g/dL)	9.4 ± 0.56	4.02 ± 0.31	6.32 ± 0.50	7.09 ± 0.82
RBC's count*#(×10^6/μL)	6.31 ± 0.64	3.01 ± 0.62	4.87 ± 0.51	5.02 ± 0.24
WBC's count*#(×10^3/μL)	3.75 ± 0.62	5.04 ± 0.51	3.98 ± 0.45	3.74 ± 0.29
ALT*# (I/U)	45.63 ± 1.16	74.56 ± 1.99	57.41 ± 1.54	49.65 ± 1.71
AST*# (I/U)	48.49 ± 0.98	89.46 ± 1.45	51.11 ± 1.65	49.85 ± 0.87
Urea*# (mg/dL)	27.32 ± 1.76	33.76 ± 1.01	28.01 ± 0.91	27.98 ± 0.85
Creatinine*# (mg/dL)	0.83 ± 0.04	1.06 ± 0.17	0.74 ± 0.06	0.62 ± 0.05

*Mean ± SEM values of mice in each group (n = **6**).
Values are significantly different (P ≤ 0.05), un-paired test using GraphPad prism.

152.3, 152.8, 160.0, 162.7; IR (KBr/cm^{-1}): 1592 (C═O), 2209 (C≡N), 2899 (NH), 3442 (NH_2); CHN Calcd. For $C_{18}H_{13}N_3O$ (287.11): C, 75.25; H, 4.56; N, 14.63. Found: C, 75.18; H, 4.47; N, 14.42%.

*3.1.1.4. 6-(4-Bromophenyl)-2-oxo-4-phenyl-1,2-dihydropyridine-3-carbonitrile **(3d)***. Yield: 66%$_{\text{DMF-Acetic acid (1:1) as white powder}}$, m.p. 294–296 °C.^{1}H NMR (400 MHz, DMSO-d_6): δ 6.9 (s, 1H), 7.58 (s, 3H), 7.74 (s, 4H), 7.87 (d, *J* = 7.6 Hz, 2H), 12.3 (s, 1H, NH); ^{13}C NMR (100 MHz, DMSO-d_6): δ 98.8, 107.3, 116.8, 125.3, 128.7, 129.2, 130.3, 130.9, 132.3, 136.5, 151.2, 160.0, 162.6, 172.4; IR (KBr/cm^{-1}): 693 (C-Br), 1609 (C═O), 2221 (C≡N), 2806 (NH); CHN Calcd. For $C_{18}H_{11}BrN_2O$ (351.2): C, 61.56; H, 3.16; Br, 22.75; N, 7.98. Found: C, 61.62; H, 3.27; Br, 22.66; N, 7.83%.

*3.1.1.5. 6-(4-Methoxyphenyl)-2-oxo-4-phenyl-1,2-dihydropyridine-3-carbonitrile **(3e)***. Yield: 47 %$_{\text{Ethanol as yellow powder}}$, m.p. 260–262 °C.^{1}H NMR (400 MHz, DMSO-d_6): δ 3.85 (s, 3H, OCH_3), 6.78 (s, 1H), 7.07 (d, *J* = 6.8 Hz, 2H), 7.57 (s, 3H), 7.72 (s, 2H), 7.90 (d, *J* = 6.8 Hz, 2H), 12.58 (s, 1H, NH);^{13}C NMR (100 MHz, DMSO-d_6): δ 56.0, 97.7, 105.7, 114.9, 117.1, 124.8, 128.6, 129.2, 129.9, 130.7, 136.8, 151.7, 160.2, 162.3, 162.5; IR (KBr/cm^{-1}): 1596 (C═O), 2217 (C≡N), 2838 (NH); CHN Calcd. For $C_{19}H_{14}N_2O_2$ (302.11): C, 75.48; H, 4.67; N, 9.27. Found: C, 75.54; H, 4.73; N, 9.08%.

*3.1.1.6. 2-Oxo-4-phenyl-1,2,5,6,7,8-hexahydroquinoline-3-carbonitrile **(3f)***. Yield: 40 %$_{\text{Ethanol as yellow powder}}$, m.p. 271–273 °C.^{1}H NMR (400 MHz, DMSO-d_6): δ1.58 (s, 2H), 1.69 (s, 2H), 2.04 (s, 2H), 2.65 (s, 2H), 7.32 (s, 2H), 7.50 (s, 3H), 12.30 (s, 1H, NH);^{13}C NMR (100 MHz, DMSO-d_6): δ 21.1, 22.3, 25.3, 27.7, 100.9, 112.8, 116.5, 127.9, 129.1, 129.4, 136.1, 150.7, 160.3, 162.3. IR (KBr/cm^{-1}): 1594 (C═O), 2224 (C≡N), 2841 (NH), 2945 (Cyclohexyl); CHN Calcd. For $C_{16}H_{14}N_2O$ (250.3): C, 76.78; H, 5.64; N, 11.19. Found: C, 76.84; H, 5.77; N, 11.04%.

*3.1.1.7. 4-(4-Methoxyphenyl)-2-oxo-6-phenyl-1,2-dihydropyridine-3-carbonitrile **(3 g)***. Yield: 38 %$_{\text{DMF-Acetic acid (1:1) as yellow powder}}$, m.p. 310–312 °C.^{1}H NMR (400 MHz, DMSO-d_6): δ3.87 (s, 3H, OCH_3), 6.80 (s, 1H), 7.12 (d, *J* = 8.0 Hz, 2H), 7.54 (d, *J* = 6.4 Hz, 3H), 7.73 (d, *J* = 8.0 Hz, 2H), 7.89 (d, *J* = 6.0 Hz, 2H), 12.60 (s, 1H, NH);^{13}C NMR (100 MHz,

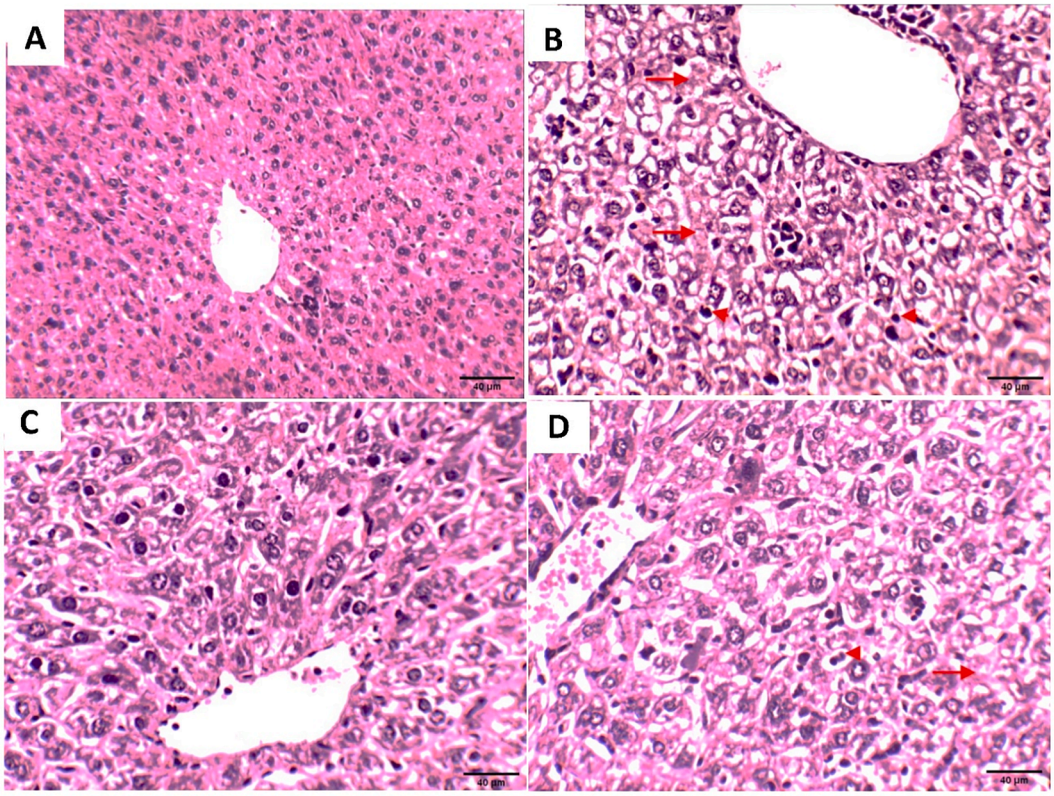

Fig. 6. Hepatic examinations of (**A**) Normal control group shows normal hepatic lobule architecture. The central vein is surrounded by hepatocyte cords. A narrow blood sinusoid is often seen between the strands of hepatocytes. (**B**) *SEC* control group shows hydropic degeneration of the hepatocytes, loss of cell boundaries and degeneration of the balloon, others hepatic cells had nuclear pyknosis (arrowheads) and karyolysis (arrows). (**C**) *SEC* mice treated with compound **4** group: shows that the hepatic lobule appears to be normal, also few hepatocytes show hydropic degeneration and activated Kupffer cells. (**D**) *SEC* mice treated with 5-FU: still exhibits hydropic degeneration of hepatocytes and nuclear pyknosis (arrowheads), and karyolysis (arrows).

Table 4
Analysis of ligand-receptor interactions with binding energies (Kcal/mol) of docked compound **7** inside two studied 4K0Y and 2OBJ as PIM-1 kinase proteins.

Protein (PDB code)	Binding affinity(Kcal/mol)	Type on interaction	Bond length (A°)	Interaction moiety involved	Amino acid
4K0Y	**−20.86**	H-acceptor	2.39	**—C≡N**	**Lys 67**
		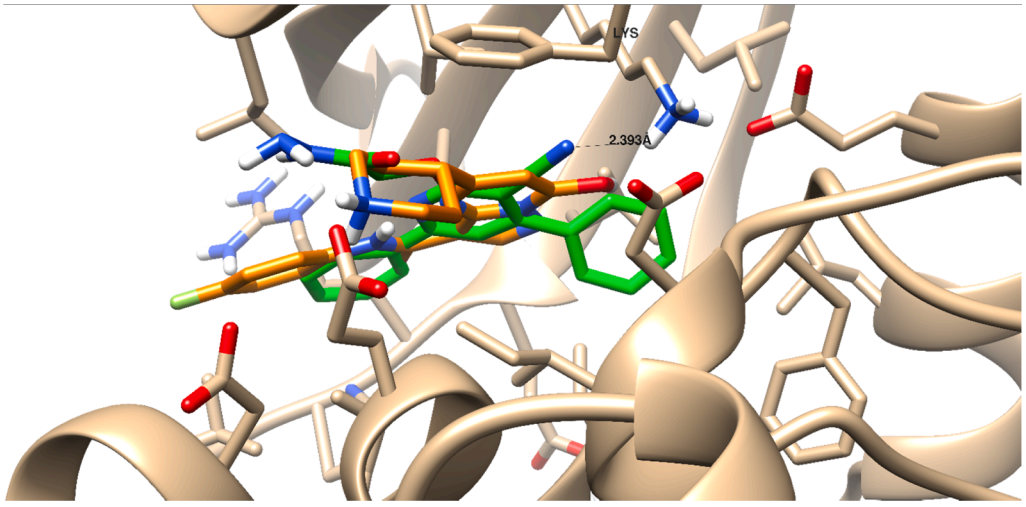			
2OBJ	**−20.70**	H-acceptor It forms arene-cation interaction with Lys 67	2.033	**—C≡N**	**Lys 67**
		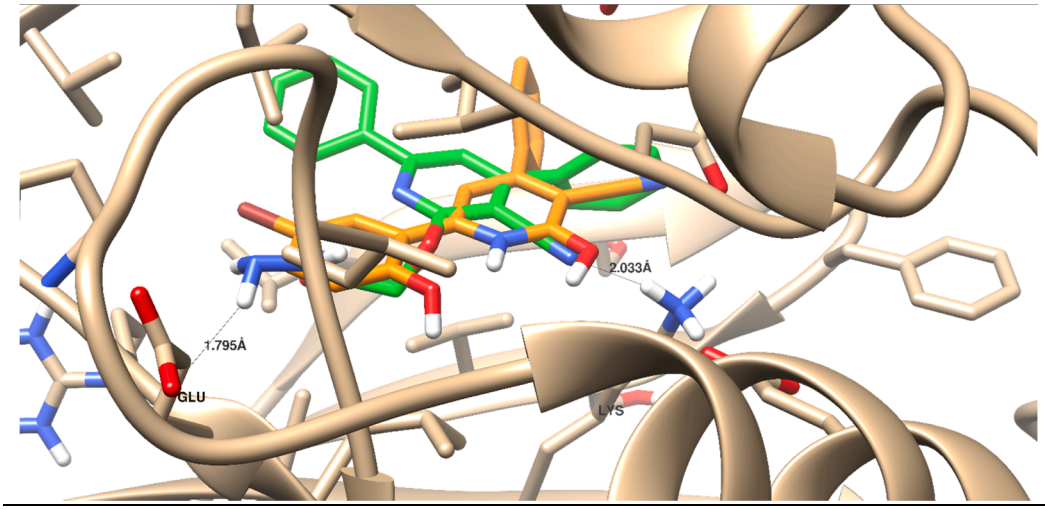			

*Superimposed compound **7** (green), and the co-crystalized ligand (Orange) inside the two studied 4K0Y and 2OBJ PIM-1 kinase protein.

DMSO-d_6): δ 55.9, 106.5, 114.7, 117.2, 128.2, 128.6, 129.3, 130.5, 131.5, 132.9, 151.6, 159.7, 161.6, 162.6; IR (KBr/cm^{-1}): 1574 (C═O), 2218 (C≡N), 2843 (NH); CHN Calcd. For $C_{19}H_{14}N_2O_2$ (302.11): C, 75.48; H, 4.67; N, 9.27. Found: C, 75.44; H, 4.62; N, 9.33; O, 10.61%.

3.1.1.8. 4-(4-Nitrophenyl)-2-oxo-6-phenyl-1,2-dihydropyridine-3-carbonitrile ***(3h)***. Yield: 41 %$_{\text{Acetic acid glacial + DMF-Ethanol (1:1) as yellow powder}}$, m. p. 300–302 °C.^{1}H NMR (400 MHz, DMSO-d_6): δ 6.93 (s, 1H), 7.57 (s, 3H), 7.94 (s, 2H), 8.00 (d, J = 7.6 Hz, 2H), 8.39 (d, J = 7.6 Hz, 2H), 12.30 (s, 1H, NH);^{13}C NMR (100 MHz, DMSO-d_6): δ 98.8, 106.7, 116.5, 124.2, 128.2, 129.3, 130.3, 131.7, 133.1, 142.9, 148.9, 153.1, 157.8, 162.6; IR (KBr/cm^{-1}): 1344, 1522 (C-NO_2), 1576 (C═O), 2218 (C≡N), 2773 (NH); CHN Calcd. For $C_{18}H_{11}N_3O_3$ (317.3): C, 68.14; H, 3.49; N, 13.24. Found: C, 68.19; H, 3.53; N, 13.35%.

3.1.1.9. 4-(3-Methoxyphenyl)-2-oxo-6-phenyl-1,2-dihydropyridine-3-carbonitrile ***(3i)***. Yield: 69 %$_{\text{Acetic acid glacial as yellow crystal}}$, m.p. 240–242 °C.^{1}H NMR (400 MHz, DMSO-d_6): δ 3.86 (s, 3H, OCH_3), 6.85 (s, 1H), 7.13 (d, J = 7.2 Hz, 1H), 7.29 (s, 2H), 7.49–7.56 (m, 4H), 7.91 (s, 2H), 12.71 (s, 1H, NH);^{13}C NMR (100 MHz, DMSO-d_6): δ 55.9, 98.8, 106.8, 114.3, 116.6, 116.7, 120.9, 128.2, 129.3, 130.4, 131.5, 133.1, 138.0, 152.2, 159.9, 162.5; IR (KBr/cm^{-1}): 1573 (C═O), 2216 (C≡N), 2836 (NH); CHN Calcd. For $C_{19}H_{14}N_2O_2$ (302.33): C, 75.48; H, 4.67; N, 9.27. Found: C, 75.51; H, 4.63; N, 9.32%.

3.1.1.10. 4-(4-(Dimethylamino)phenyl)-2-oxo-6-phenyl-1,2-dihydropyridine-3-carbonitrile ***(3j)***. Yield: 44 %$_{\text{Ethanol as yellow powder}}$, m.p. 260–262 °C.^{1}H NMR (400 MHz, DMSO-d_6): δ 3.03 (s, 6H, $N(CH_3)_2$), 6.84 (s, 1H), 6.85 (d, J = 7.6 Hz, 2H), 7.55 (s, 3H), 7.69 (d, J = 8.0 Hz, 2H), 7.87 (s, 2H), 12.50 (s, 1H, NH);^{13}C NMR (100 MHz, DMSO-d_6): $\delta \approx$ 39.6, 105.9, 112.1, 117.8, 122.7, 128.0, 129.3, 130.1, 131.1, 133.1, 152.4, 159.8, 162.9; IR (KBr/cm^{-1}): 1598 (C═O), 2213 (C≡N), 2792 (NH); CHN Calcd. For $C_{20}H_{17}N_3O$ (315.14): C, 76.17; H, 5.43; N, 13.32. Found: C, 76.21; H, 5.47; N, 13.39%.

3.1.1.11. 4-(Furan-2-yl)-2-oxo-6-phenyl-1,2-dihydropyridine-3-carbonitrile ***(3 k)***. Yield: 35 %$_{\text{Ethanol-acetic acid (1:1) as brown crystal}}$, m.p. 300 °C.^{1}H NMR (400 MHz, DMSO-d_6): δ 6.85 (s, 1H), 7.05 (s, 1H), 7.57 (s, 3H), 7.71 (s, 1H), 7.88 (s, 2H), 8.09 (s, 1H), 12.54 (s, 1H, NH);^{13}C NMR (100 MHz, DMSO-d_6): δ 93.0, 101.5, 113.8, 116.7, 117.1, 128.1, 129.4, 131.6, 132.8, 145.6, 147.5, 148.3, 151.8, 162.6; IR (KBr/cm^{-1}): 1570 (C═O), 2773–2892 furyl ring, 2214 (C≡N), 2773 (NH); CHN Calcd. For

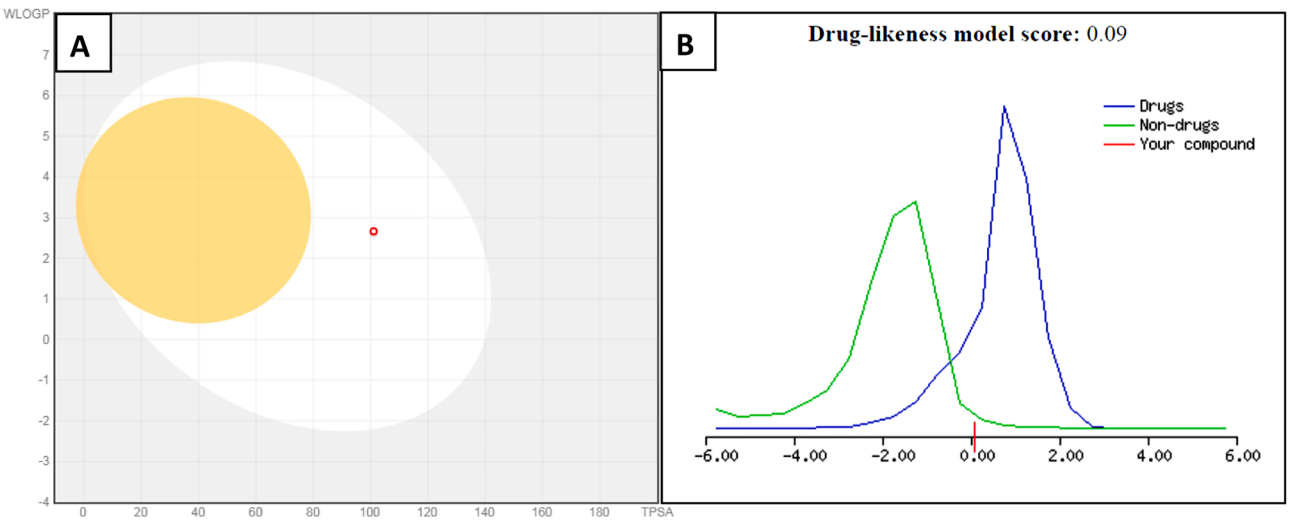

Fig. 7. A: BOILED-Egg model for compound **7** using SwissADME "points located in the BOILED-Egg's yolk are molecules predicted to passively permeate through the blood–brain barrier (BBB), while points located in the BOILED-Egg's white are molecules predicted to be passively absorbed by Gastrointestinal (GI) tract GI", **B:** Drug likeness score of compound **7** using MolSoft "The green color means non-drug like behavior and those fall under blue color area are considered as drug-like. Those compounds having negative or zero value should not be considered as drug like" (For interpretation of the references to color in this figure legend, the reader is referred to the web version of this article.)

Table 5
Molecular properties of and drug-likeness.

Website	CompoundADME	7	13a	13c
molinspiration 2018.10	Mwt (D)	344.37	401.42	415.45
	MV (A^3)	308.02	358.07	374.87
	PSA (A^2)	101.04	101.32	101.32
	Log p	2.07	3.38	3.35
	nrotb	5	8	9
	nviolations	0	0	0
MolSoft	HBA	5	6	6
	HBD	3	1	1
	Solubility (mg/L)	78.72	29.63	42.77
	Drug-likeness score	0.09	0.08	0.12

MWt: Molecular Weight, MV: Molecular Volume, PAS: Polar Surface Area, Log p: Log P: Octanol-water partition coefficient, nrotb: number of rotatable bond, nviolations: number of violations, HBA: Hydrogen Bond Acceptor, HBD: Hydrogen Bond Donor.

$C_{16}H_{10}N_2O_2$ (262.26): C, 73.27; H, 3.84; N, 10.68. Found: C, 73.73; H, 3.91; N, 10.49%.

3.1.1.12. 4-(3-Chlorophenyl)-6-(4-chlorophenyl)-2-oxo-1,2-dihydropyridine-3-carbonitrile ***(3l)***. Yield: 55%$_{\text{Ethanol as yellow powder,}}$m.p. 302–304 °C.^{1}H NMR (400 MHz, DMSO-d_6): δ 7.08 (s, 1H), 7.61 (d, J = 8.0 Hz, 2H), 7.87 (t, J = 8.0 Hz, 1H), 7.98 (d, J = 7.2 Hz, 2H), 8.19 (d, J = 8.0 Hz, 1H), 8.41 (d, J = 8.4 Hz, 1H), 8.56 (s, 1H), 12.9 (s, 1H, NH);^{13}C NMR (100 MHz, DMSO-d_6): δ 116.4, 123.7, 125.4, 129.4, 130.2, 131.0, 135.4, 136.6, 137.9, 148.4; IR (KBr/cm^{-1}): 689 (C-Cl), 1600 (C═O), 2216 (C≡N), 2956 (NH); CHN Calcd. For $C_{18}H_{10}Cl_2N_2O$ (341.19): C, 63.37; H, 2.95; Cl, 20.78; N, 8.21. Found: C, 63.33; H, 3.01; Cl, 20.83; N, 8.29%.

3.1.1.13. 6-(4-Chlorophenyl)-4-(4-methoxyphenyl)-2-oxo-1,2-dihydropyridine-3-carbonitrile ***(3m)***. Yield: 51%$_{\text{Ethanol as yellowish white powder,}}$m.p. 275–277 °C.^{1}H NMR (400 MHz, DMSO-d_6): δ 3.87 (s, 3H), 6.87 (s, 1H), 7.12 (d, J = 8.4 Hz, 2H), 7.59 (d, J = 8.4 Hz, 2H), 7.73 (d, J = 8.4 Hz, 2H), 7.94 (d, J = 8.0 Hz, 2H), 12.65 (s, 1H, NH);^{13}C NMR (100 MHz, DMSO-d_6): δ 56.0, 114.8, 129.3, 130.0, 130.4; IR (KBr/cm^{-1}): 689 (C-Cl), 1656 (C═O), 2200 (C≡N), 3413 (NH); CHN Calcd. For $C_{19}H_{13}ClN_2O_2$ (336.78): C, 67.76; H, 3.89; Cl, 10.53; N, 8.32. Found: C, 67.71; H, 3.91; Cl, 10.49; N, 8.25%.

3.1.1.14. 6-(3-Aminophenyl)-4-(4-methoxyphenyl)-2-oxo-1,2-dihydropyridine-3-carbonitrile ***(3n)***. Yield: 59 %$_{\text{Acetic acid glacial as white powder,}}$ m.p. 300–302 °C.^{1}H NMR (400 MHz, DMSO-d_6): δ 3.86 (s, 3H), 5.27 (s, 1H), 6.61 (s, 1H), 6.76 (d, J = 6.8 Hz, 1H), 7.01 (s, 2H), 7.11–7.17 (m, 4H), 7.70 (d, J = 6.8 Hz, 2H), 12.30 (s, 1H, NH);^{13}C NMR (100 MHz, DMSO-d_6): δ 98.8, 106.8, 114.2, 116.6, 116.7, 120.9, 128.2, 129.3, 130.4, 131.5, 133.1, 138.0, 152.2, 159.9, 162.5; IR (KBr/cm^{-1}): 1600 (C═O), 2218 (C≡N), 2903 (NH), 3140 (NH_2); CHN Calcd. For $C_{19}H_{15}N_3O_2$ (317.35): C, 71.91; H, 4.76; N, 13.24. Found: C, 71.87; H, 4.72; N, 13.29%.

3.1.2. Coupling of 3a with a set of alkyl halides:

To a mixture of pyridone **3a** (1.0 mol), K_2CO_3 (1.2 mol) in acetone 10 mL and DMF 1.0 mL, the appropriate alkyl halide (1.1 mol) (named benzyl chloride, phenacyl bromide and ethyl chloroacetate) was added. The mixture was refluxed for 5 h, cooled, poured into ice water filtered, dried and recrystallized in ethanol.

3.1.2.1. 2-(benzyloxy)-4,6-diphenylnicotinonitrile (4). Yield: 70% $_{\text{as yellowish white powder,}}$ m.p. 140–142 °C.^{1}H NMR (400 MHz, DMSO-d_6): δ 5.70 (s, 2H), 7.36–7.82 (m, 14H), 8.27 (s, 2H); ^{13}C NMR (100 MHz, DMSO-d_6): δ 68.8, 93.0, 114.5, 115.7, 128.0, 128.3, 128.5, 129.0, 129.1, 129.3, 129.4, 130.5, 131.2, 136.3, 137.0, 137.1, 157.0, 157.8, 164.2; IR (KBr /cm^{-1}): 2195 (C≡N); CHN Calcd. For $C_{25}H_{18}N_2O$ (362.14): C, 82.39; H, 5.53; N, 7.69. Found: C, 82.32; H, 5.57; N, 7.61%.

3.1.2.2. 2-(2-Oxo-2-phenylethoxy)-4,6-diphenylnicotinonitrile (5). Yield:

Table 6
Molinspiration bioactivity scores for compounds **7.**

Compound	GPCR ligand	Ion channel modulator	Kinase inhibitor	Nuclear receptor ligand	Protease inhibitor	Enzyme inhibitor
7	−0.11	−0.34	**0.11**	−0.28	−0.15	0.02

90% as yellowish white powder, m.p.166–168 °C.^{1}H NMR (400 MHz, DMSO-d_6): δ 6.0 (s, 2H), 7.33 (t, J = 7.5 Hz, 2H), 7.41 (t, J = 7.2 Hz, 1H), 7.61–7.82 (m, 9H), 7.98 (d, J = 7.2 Hz, 2H), 8.08 (d, J = 7.2 Hz, 2H); ^{13}C NMR (100 MHz, DMSO-d_6): δ 69.3, 92.7, 114.8, 115.6, 127.8, 128.2, 128.3, 128.7, 129.1, 129.2, 129.4, 130.6, 130.8, 131.1, 132.9, 135.0, 136.2, 136.6, 136.8, 157.1, 157.5, 163.6, 194.3; IR (KBr/cm^{-1}): 1587 (C═O), 2219 (C≡N); CHN Calcd. For $C_{26}H_{18}N_2O_2$ (390.44): C, 79.98; H, 4.65; N, 7.17. Found: C, 79.93; H, 4.59; N, 7.23%.

3.1.2.3. Ethyl 2-(3-cyano-4, 6-diphenylpyridin-2-yloxy)acetate (6). Yield: 60% as white powder, m.p.138–140 °C.^{1}H NMR (400 MHz, DMSO-d_6): δ 1.22 (t, ***J*** = 7.0 Hz, 3H, CH_3), 4.2 (q, ***J*** = 6.9 Hz, 2H, CH_2), 5.18 (s, 2H), 7.53 (s, 3H), 7.60 (s, 3H), 7.77 (s, 2H), 7.87 (s, 1H), 8.18 (s, 2H); ^{13}C NMR (100 MHz, DMSO-d_6): δ 14.5, 61.2, 64.2, 92.7, 114.9, 115.4, 127.8, 129.1, 129.3, 130.6, 131.3, 136.1, 136.6, 157.1, 157.3, 163.4, 168.7; IR (KBr/cm^{-1}): 1590 (C═O), 2224 (C≡N); CHN Calcd. For $C_{22}H_{18}N_2O_3$ (358.40): C, 73.73; H, 5.06; N, 7.82. Found: C, 73.79; H, 4.99; N, 7.85%.

3.1.3. Hydrazinolysis of the ester 6:

3.1.3.1. 2-(3-Cyano-4,6-diphenylpyridin-2-yloxy)acetohydrazide (7). To the ester **6** (1.0 mol) in MeOH (20 mL), hydrazine hydrate (3.0 mol) was added and the mixture was refluxed for 3.5 h then left to cool. The formed precipitate was filtered, washed with water, dried and recrystallized from ethanol.

Yield: 50% as yellowish white powder, m.p. 204 °C.^{1}H NMR (400 MHz, DMSO-d_6): δ 4.30 (s, 2H), 5.03 (s, 2H), 7.50–8.28 (m, 11*H*), 9.39 (s, 1 H); ^{13}C NMR (100 MHz, DMSO-d_6): δ 64.9, 93.2, 114.7, 115.7, 128.0, 129.1, 129.4, 130.6, 131.2, 136.3, 136.9, 156.9, 157.5, 163.8, 167.0; IR (KBr/cm^{-1}): 1604 (C═O), 2216 (C≡N), 2731 (NH), 3291 (NH_2); CHN Calcd. For $C_{20}H_{16}N_4O_2$ (344.37): C, 69.76; H, 4.68; N, 16.27. Found: C, 69.80; H, 4.65; N, 16.35%

3.1.3.2. Heterocyclization of hydrazide (7). To a mixture of hydrazide **7** (1.1 mmol, 0.5 g) in ethanol 10 mL, KOH (0.4 g in 0.5 mL water) and carbon disulphide (2.0 mL) were added and stirred overnight then diethyl ether 10.0 mL was added and stirred for additional 6 h, the excess solvent was evaporated, distilled water was added and the mixture was acidified with conc. HCl, the formed solid was filtered, washed with water, dried and recrystallized from ethanol to give **8**. When the mixture was refluxed with stirring for **7** h followed by solvent evaporation, acidification and recrystallization compound **9** was obtained.

3.1.3.3. 2-(2-((3-Cyano-4,6-diphenylpyridin-2-yl)oxy)acetyl)hydrazine-1-carbodithioic acid (8). Yield: 60% as brownish red powder, m.p. 95–97 °C.^{1}H NMR (400 MHz, DMSO-d_6): δ 3.54 (s, 1H, SH), 5.64 (s, 2H), 7.54–7.61 (m, 8H), 7.73–7.79 (m, 2H), 7.87 (s, 1H), 8.28–8.31 (m, 2H);^{13}C NMR (100 MHz, DMSO-d_6): δ 59.0, 92.9, 115.0, 115.4, 128.1, 128.7, 129.1, 129.3, 129.4, 130.6, 130.9, 131.3, 136.2, 136.8, 136.8, 157.3, 157.7, 159.1, 163.3, 180.5;IR (KBr/cm^{-1}): 759 (C—S), 1561 (C═O), 1628 (C═S), 2250 (C≡N), 3416, 3460 (CO-NH); CHN Calcd. For $C_{21}H_{16}N_4O_2S_2$ (420.51): C, 59.98; H, 3.84; N, 13.32; S, 15.25. Found: C, 59.93; H, 3.87; N, 13.28; S, 15.34%.

3.1.3.4. 4,6-Diphenyl-2-((5-thioxo-4,5-dihydro-1,3,4-oxadiazol-2-yl) methoxy)nicotinonitrile (9). Yield: 80% as yellow orange powder, m.p. 215 °C.^{1}H NMR (400 MHz, DMSO-d_6): δ 5.77 (s, 2H), 7.54–7.62 (m, 6H), 7.77–7.80 (m, 2H), 7.93 (s, 1H), 8.25–8.27 (m, 2H), 14.64 (br.s, 1H, NH);^{13}C NMR (100 MHz, DMSO-d_6): δ 58.7, 93.2, 115.1, 115.5, 128.0, 128.6, 129.1, 129.2, 129.3, 129.4, 130.6, 130.7, 131.3, 131.5, 136.1, 136.7, 157.4, 157.7, 159.9, 162.9, 178.7; IR (KBr/cm^{-1}): 695 (C—S), 1598 (C═O), 1641 (C═N), 2218 (C≡N); CHN Calcd. For $C_{21}H_{14}N_4O_2S$ (344.37): C, 65.27; H, 3.65; N, 14.50; S, 8.30. Found: C, 65.32; H, 3.69; N, 14.41; S, 8.36%.

3.1.3.5. 2-((5-((2-Oxo-2-phenylethyl)thio)-1,3,4-oxadiazol-2-yl) methoxy)-4,6-diphenylnicotinonitrile (10). A mixture of oxadiazolethione **9** (1.0 mmol), potassium carbonate and phenacyl bromide in acetone/DMF 10:1 was heated under reflux for 3 h cooled, poured into water filtered, dried and recrystallized from MeOH to give **(10)**;

Yield: 70% as yellow brown powder, m.p. 92–94 °C.^{1}H NMR (400 MHz, DMSO-d_6): δ 5.1 (s, 2H), 5.9 (s, 2H), 7.54–7.68 (m, 8H), 7.76 (s, 3H), 7.89 (s, 1H), 7.99 (d, J = 7.2 Hz, 2H), 8.24 (s, 2H);^{13}C NMR (100 MHz, DMSO-d_6): δ 39.7, 58.6, 93.1, 115.1, 115.4, 128.0, 128.8, 129.1, 129.3, 130.6, 131.3, 134.3, 135.6, 136.2, 136.8, 157.4, 157.7, 163.0, 164.1, 164.6, 192.8; CHN Calcd. For $C_{29}H_{20}N_4O_3S$ (504.56): C, 69.03; H, 4.00; N, 11.10; S, 6.35. Found: C, 69.09; H, 3.97; N, 11.15; S, 6.32%.

3.1.3.6. Coupling of 2-(3-cyano-4,6-diphenylpyridin-2-yloxy)aceto hydrazide(7) with amines (12a-e) and α-Amino acid ester (13a,b):. To a cold solution (∼−5°C) of hydrazide **7** (0.01 mmol) in 1.0 N HCl (20 mL) and acetic acid 96% (3 mL), 5 mL aqueous solution of $NaNO_2$ (0.02 mmol) was added to the mixture dropwise, then the mixture was stirred at 0 °C for 30 min. The reaction mixture was extracted three times with 30.0 mL ethyl acetate. The extract was washed several times with 3% aqueous solution of Na_2CO_3 till it became neutral then washed with water. The azide extract **11** was dried over Na_2SO_4. The azide solution **11** was allowed to react with appropriate amines (*N*-propyl amine, benzyl amine, tetradecyl amine, allyl amine and pipyridine) or selected amino ester hydrochloride (0.01 mol) (glycine and L-leucine) in the presence of triethyl amine (1.0 mL, 0.01 mol) after complete addition, the reaction mixture was kept at −5°C for 24 h, and then at room temperature for another 24 h. The reaction mixture washed with 0.5 N HCl, water, 3% solution of Na_2CO_3, and dried over Na_2SO_4. The solution was evaporated to dryness, and the residues were recrystallized by ethyl acetate/petroleum ether 1:1 to give the desired product.

3.1.3.7. 2-(3-Cyano-4,6-diphenylpyridin-2-yloxy)-N-propylacetamide (12a). Yield: 80% as white powder, m.p. 180–182 °C.^{1}H NMR (400 MHz, DMSO-d_6): δ 0.82 (t, J = 6.0 Hz, 3H), 1.42–1.45 (m, 2H), 3.20 (m, 2H), 5.00 (s, 2H), 7.53–8.23 (m, 12H); ^{13}C NMR (100 MHz, DMSO-d_6): δ 11.8, 22.9, 65.9, 93.0, 114.5, 115.7, 128.0, 129.1, 129.3, 129.4, 130.6, 131.2, 136.3, 136.9, 156.9, 157.4, 163.9, 167.5;IR (KBr/cm^{-1}): 1589 (C═O), 2219 (C≡N), 2875 (NH); CHN Calcd. For $C_{23}H_{21}N_3O_2$ (371.44): C, 74.37; H, 5.70; N, 11.31. Found: C, 74.31; H, 5.75; N, 11.29%.

3.1.3.8. N-benzyl-2-(3-cyano-4,6-diphenylpyridin-2-yloxy)acetamide (12b). Yield: 30% as white powder, m.p. 183–185 °C.^{1}H NMR (400 MHz, DMSO-d_6): δ 4.35 (d, J = 6.0 Hz, 2H), 5.11 (s, 2H), 7.10–7.15 (m, 3H), 7.20 (d, J = 7.2 Hz, 2H), 7.50–7.53 (m, 3H), 7.61–7.62 (m, 2H), 7.77 (m, 2H), 7.86 (s, 1H), 8.22 (d, J = 7.2 Hz, 1H), 8.67 (m, 1H); ^{13}C NMR (100 MHz, DMSO-d_6): δ 42.4, 65.9, 93.2, 114.7, 115.7, 127.1, 127.5, 127.7, 128.0, 128.5, 129.1, 129.3, 130.6, 131.2, 136.3, 136.9, 139.6, 156.9, 157.6, 163.9, 167.8;IR (KBr/cm^{-1}): 1584 (C═O), 2217 (C≡N), 2911 (NH); CHN Calcd. For $C_{27}H_{21}N_3O_2$ (419.48): C, 77.31; H, 5.05; N, 10.02. Found: C, 77.26; H, 4.97; N, 10.13%.

3.1.3.9. 2-(3-Cyano-4,6-diphenylpyridin-2-yloxy)-N-tetradecylacetamide (12c). Yield: 50% as white powder, m.p. 138–140 °C.^{1}H NMR (400 MHz, DMSO-d_6): δ 0.85 (t, J = 5.6 Hz, 3H), 1.15–1.25 (m, 24H), 3.28 (m, 2H), 4.98 (s, 2H), 7.52–8.24 (m, 12H); ^{13}C NMR (100 MHz, DMSO-d_6): δ 14.3, 22.5, 26.8, 29.1, 29.4, 31.7, 40.7, 127.1, 127.5, 128.0, 129.0, 129.2, 129.4, 131.2;IR (KBr/cm^{-1}): 1589 (C═O), 2200 (C≡N), 2848 (NH); CHN Calcd. For $C_{34}H_{43}N_3O_2$ (525.74): C, 77.68; H, 8.24; N, 7.99. Found: C, 77.71; H, 8.19; N, 7.93%.

3.1.3.10. N-allyl-2-(3-cyano-4,6-diphenylpyridin-2-yloxy)acetamide (12d). Yield: 48% as white powder, m.p. 153–155 °C.^{1}H NMR (400 MHz,

DMSO-d_6): δ 3.79–3.87 (m, 3H), 4.99–5.18 (m, 4H), 5.77–5.84 (m, 1H), 7.53–8.23 (m, 11*H*); ^{13}C NMR (100 MHz, DMSO-d_6): δ 41.2, 65.8, 93.1, 114.6, 115.8, 128.0, 129.0, 129.3, 130.6, 131.2, 135.5, 136.3, 136.9, 157.0, 157.5, 163.9, 167.5;IR (KBr/cm^{-1}): 1588 (C═O), 2220 (C≡N), 3287 (NH); CHN Calcd. For $C_{23}H_{19}N_3O_2$ (369.42): C, 74.78; H, 5.18; N, 11.37. Found: C, 74.71; H, 5.23; N, 11.33%.

3.1.3.11. 2-(2-Oxo-2-(piperidin-1-yl)ethoxy)-4,6-diphenylnicotinonitrile (12e). Yield: 75% as white powder, m.p. 208–210 °C.^{1}H NMR (400 MHz, DMSO-d_6): δ 1.47–1.66 (m, 6H), 3.48 (d, J = 8.0H, 4H), 5.35 (s, 2H), 7.53–8.20 (m, 11*H*); ^{13}C NMR (100 MHz, DMSO-d_6): δ 24.5, 25.8, 26.5, 42.8, 45.5, 64.6, 92.7, 114.4, 115.7, 127.9, 129.1, 129.3, 129.4, 130.6, 131.2, 136.3, 137.0, 156.9, 157.4, 164.1, 165.2;IR (KBr/cm^{-1}): 1587 (C═O), 2218 (C≡N), 2856 (NH); CHN Calcd. For $C_{25}H_{23}N_3O_2$ (397.48): C, 75.55; H, 5.83; N, 10.57. Found: C, 75.51; H, 5.86; N, 10.55%.

3.1.3.12. Reaction of 2-(3-cyano-4,6-diphenylpyridin-2-yloxy)acetohydrazide (7) with α-amino acids esters to give(13a-b)

3.1.3.12.1. Methyl 2-(2-(3-cyano-4,6-diphenylpyridin-2-yloxy)acetamido)acetate (13a). Yield: 30% as white crystal, m.p. 188–190 °C.^{1}H NMR (400 MHz, DMSO-d_6): δ 3.60 (s, 3H), 3.94 (d, J = 5.6 Hz, 2H), 5.11 (s, 2H), 7.51–7.78 (m, 6H), 7.85 (s, 1H), 8.23–8.61 (m, 4H), 13.66 (s, 1H); ^{13}C NMR (100 MHz, DMSO-d_6): δ 52.1, 55.9, 65.4, 93.0, 114.5, 114.7, 117.4, 118.2, 128.0, 129.3, 129.6, 130.0, 130.6, 131.2, 135.5, 132.3, 136.9, 157.4, 157.5, 165.9, 169.7, 170.5; IR (KBr/cm^{-1}): 1587 (C═O), 2220 (C≡N), 2905 (NH); CHN Calcd. For $C_{23}H_{19}N_3O_4$ (401.42): C, 68.82; H, 4.77; N, 10.47. Found: C, 68.79; H, 4.73; N, 10.51%.

3.1.3.12.2. Methyl 2-(2-(3-cyano-4,6-diphenylpyridin-2-yloxy)acetamido)-4-methyl pentanoate (13b). Yield: 30% as Yellowish white powder, m.p. 118–120 °C.^{1}H NMR (400 MHz, DMSO-d_6): δ 0.71 (d, J = 6.0 Hz, 3H), 0.76 (d, J = 6.0 Hz, 3H), 1.52–1.59 (m, 1H), 3.58 (s, 3H), 4.39 (q, J = 6.0 Hz, 1H), 4.99 (s, 2H), 5.03–5.15 (m, 2H), 7.29 (s, 1H), 7.51–7.78 (m, 5H), 7.84 (s, 2H), 8.21–8.25 (m, 2H), 8.60 (d, J = 8.0 Hz, 1H); ^{13}C NMR (100 MHz, DMSO-d_6): δ 21.6, 23.1, 24.5, 50.4, 52.3, 65.4, 65.5, 92.9, 93.0, 114.6, 115.7, 128.0, 128.7, 129.1, 130.3, 130.7, 131.2, 132.3, 135.5, 136.8, 137.0, 156.9, 157.5, 163.8, 167.8, 169.7, 173.2;IR (KBr/cm^{-1}): 1586 (C═O), 2221 (C≡N), 2953 (NH); CHN Calcd. For $C_{27}H_{27}N_3O_4$ (457.53): C, 70.88; H, 5.95; N, 9.18. Found: C, 70.91; H, 5.91; N, 9.12%.

3.2. Biological assays

3.2.1. Cell culture, treatment and MTT assay

The human liver carcinoma cell line (HepG2), and normal liver cells (THLE2) were purchased from the National Cancer Institute, Cairo, Egypt. Cells were maintained in DMEM media supplemented with 2mML-glutamine (Lonza, Belgium) and 10% FBS (Sigma, St. Louis, MO, USA), 1% Penicillin/Streptomycin (Lonza, Belgium) according to the routine culture work [36]. Cells after culturing were treated with the indicated compounds at the indicated concentrations (0.01, 0.1, 1, 10, and 100 μM). Cell viability was assessed after 48 h using MTT solution (Promega) [37]. Absorbance was subsequently measured (570 nm) using a plate reader, then percentages of cell viabilities at corresponding concentrations were recorded and the IC_{50} values were calculated using GraphPad Prism 7 software [38–40].

3.2.2. Annexin V/PI and cell cycle analysis

Apoptosis rate in cells was quantified using annexin V-FITC (BD Pharmingen, USA). Cells were seeded into 6-well culture plates (3–5 × 105 cells/well) and cultured as routine work. Cells were then treated with compound **7** (IC_{50} = 7.26 μM, 48 h), and cells were collected and washed with ice-cold PBS. Next, cells were suspended in 100 μL of annexin binding buffer solution "25 mM CaCl2, 1.4 M NaCl, and 0.1 M Hepes/NaOH, pH 7.4, and incubated in the dark for 30 min with annexin V-FITC solution (1:100)and PI at 10 μg/mL concentration". Stained cells and Cell cycle distribution were then acquired by Cytoflex FACS machine. Flow cytometric methodologies (annexin V/PI staining with cell cycle analyses**)** are carried out as previously described in [22,28,29].

3.2.3. RT-PCR

HepG2 cells were treated with compound**7** (IC_{50} = 7.26 μM, 48 h). At the end of treatments, cells were collected, RNA was extracted, cDNA was synthesized and Real-time RT-PCR reactions were performed following the manufacturer's instructions and our previous publications [39–42]. Then, The Ct values were collected, and the relative folds of changes between all the samples. Primers sequnces in both forward and reverse directions are summarized in Table 7.

3.2.4. In vivo (SEC animal model)

All protocols and procedures employed in animal studies were suumarized in Fig. 8, and were ethically reviewed and approved by Suez Canal University's Ethical Committee (REC-07-2020).

3.2.5. In silico studies

3.2.5.1. Molecular docking simulation. For elucidation, the virtual mechanism of binding, the molecular docking study towards the Pim-1 kinase active site was carried out. All synthesized derivatives were chemically and energetically optimized. Additionally, protein structures (PDB = 2OBJ, 4K0Y) were freely accessible from the PDB and optimized following the routine work as discussed by Nafie *et* al [43]. MOE 2019 was used as the validated molecular docking calculation, and Chimera software was finally used as the visualized software for the analysis of drug-target interactions.

3.2.5.2. ADME pharmacokinetics. In silico ADME pharmacokinetics parameters of the most active compounds were calculated using a set of software including "MolSoft", "Molinspiration", and "SwissADME" websites as previously described by Youssef et al., 2020 [29,44].

4. Conclusion

In summary, a series of **14** derivatives of 4,6-diaryl-3-cyano-2-pyridones **3a-n** were synthesized from various aromatic aldehydes, ketones, ethyl cyanoacetate, and ammonium acetate in butanol. Alkylation of pyridones was found to proceed on oxygen. Alkylation of 1,3,4-oxadiazolethione was deduced to occur on sulfur. Azide-coupling method was found to couple the hydrazide **7** with a set of amines and amino acid esters HCl. Compound **7** give the most cytotoxic activity against HepG2 with the lowest IC_{50} value of 7.26 compared to 5-FU (IC_{50} = 6.98 μM),

Table 7
Primers used for real-time RT-PCR.

Primer	Sequence
β-Actin	FOR: 5′-GCACTCTTCCAGCCTTCCTTCC-3′REV: 5′-GAGCCGCCGATCCACACG-3′
P53	FOR: 5′-CTTTGAGGTGCGTGTTTGTG-3′REV: 5′-GTGGTTTCTTCTTTGGCTGG-3′
Bcl-2	FOR: 5′-GAGGATTGTGGCCTTCTTTG-3′REV: 5′-ACAGTTCCACAAAGGCATCC-3′
PUMA	FOR: 5′-GAGGAGGAACAGTGGGC-3′REV: 5′-CTAATTGGGCTCCATCTCGG-3′
BAX	FOR: 5′-TTTGCTTCAGGGTTTCATCC-3′REV: 5′-CAGTTGAAGTTGCCGTCAGA-3′
Casp-3	FOR: 5′-TGGCCCTGAAATACGAAGTC-3′REV: 5′-GGCAGTAGTCGACTCTGAAG-3′
Casp-8	FOR: 5′-AATGTTGGAGGAAAGCAAT-3′REV: 5′-CATAGTCGTTGATTATCTTCAGC-3′
Casp-9	FOR: 5′-CGAACTAACAGGCAAGCAGC-3′REV: 5′-ACCTCACCAAATCCTCCAGAAC-3′
PIM-1	FOR: 5′-GCAAATAGCAGCCTTTCTGG-3′REV: 5′-CCTAGGACCCCTGGAGAGTC-3′

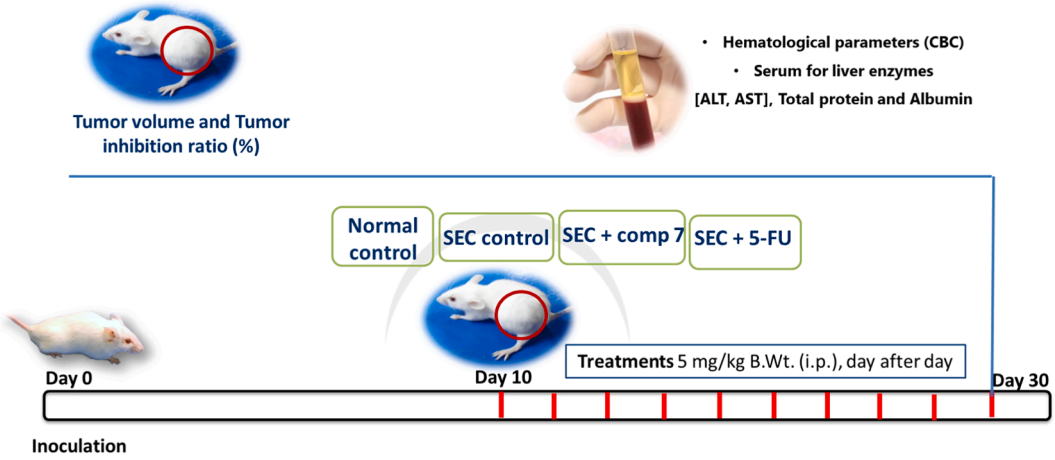

Fig. 8. *In vivo* experiment design [28,29]

and it was nontoxic against THLE2 cells. It inhibited cell growth by 76.76%. Additionally, it significantly stimulated apoptotic liver cancer cell death with 49.78-fold (22.90% compared to 0.46% for the control) arresting cell cycle pre-G1 with 35.16% population, compared to 1.57% for the control. Moreover, it validated the intrinsic apoptosis through upregulation of P53, and other related genes, with inhibition of anti-apoptotic genes through PIM-1 inhibition. Hence, this compound is worthy to be tested preclinically and further developed as a chemo-therapeutic anti-cancer drug.

Declaration of Competing Interest

The authors declare that they have no known competing financial interests or personal relationships that could have appeared to influence the work reported in this paper.

References

[1] F. Bray, J. Ferlay, I. Soerjomataram, R.L. Siegel, L.A. Torre, A. Jemal, Global cancer statistics 2018: GLOBOCAN estimates of incidence and mortality worldwide for 36 cancers in 185 countries, CA: A Cancer J. Clin. 68 (6) (2018) 394–424, https://doi.org/10.3322/caac.v68.610.3322/caac.21492.

[2] P. Dasgupta, C. Henshaw, D.R. Youlden, P.J. Clark, J.F. Aitken, P.D. Baade, Global Trends in Incidence Rates of Primary Adult Liver Cancers: A Systematic Review and Meta-Analysis, Front. Oncol. 10 (2020), https://doi.org/10.3389/fonc.2020.0017110.3389/fonc.2020.00171.s00110.3389/fonc.2020.00171.s00210.3389/fonc.2020.00171.s00310.3389/fonc.2020.00171.s004.

[3] B.T. Le, M. Kumarasiri, J.RJ. Adams, M. Yu, R. Milne, M.J. Sykes, S. Wang, Targeting Pim kinases for cancer treatment: opportunities and challenges, Future Med. Chem. 7 (1) (2015) 35–53, https://doi.org/10.4155/fmc.14.145.

[4] J. Domen, N.M. van der Lugt, D. Acton, P.W. Laird, K. Linders, A. Berns, Pim-1 levels determine the size of early B lymphoid compartments in bone marrow, J. Exp. Med. 178 (1993) 1665–1673, https://doi.org/10.1084/jem.178.5.1665.

[5] N. An, A.S. Kraft, Y. Kang, Abnormal hematopoietic phenotypes in Pim kinase triple knockout mice, J. Hematol. Oncol. 6 (1) (2013) 12, https://doi.org/10.1186/1756-8722-6-12.

[6] T. Mochizuki, C. Kitanaka, K. Noguchi, T. Muramatsu, A. Asai, Y. Kuchino, Physical and functional interactions between Pim-1 kinase and Cdc25A phosphatase. Implications for the Pim-1-mediated activation of the c-Myc signaling pathway, J. Biol. Chem. 274 (26) (1999) 18659–18666, https://doi.org/10.1074/jbc.274.26.18659.

[7] J. Li, X.F. Hu, B.E. Loveland, P.X. Xing, Pim-1 expression and monoclonal antibody targeting in human leukemia cell lines, Exp. Hematol. 37 (11) (2009) 1284–1294, https://doi.org/10.1016/j.exphem.2009.08.002.

[8] Y. Xie, K. Xu, D.E. Linn, X.i. Yang, Z. Guo, H. Shimelis, T. Nakanishi, D.D. Ross, H. Chen, L. Fazli, M.E. Gleave, Y. Qiu, The 44-kDa Pim-1 kinase phosphorylates BCRP/ABCG2 and thereby promotes its multimerization and drug-resistant activity in human prostate cancer cells, J. Biol. Chem. 283 (6) (2008) 3349–3356, https://doi.org/10.1074/jbc.M707773200.

[9] H.T. Cuypers, G. Selten, A. Berns, A.H.M. Geurts van Kessel, Assignment of the human homologue of Pim-1, a mouse gene implicated in leukemogenesis, to the pter-q12 region of chromosome 6, Hum. Genet. 72 (3) (1986) 262–265, https://doi.org/10.1007/BF00291892.

[10] A. Valdman, X. Fang, S.-T. Pang, P. Ekman, L. Egevad, Pim-1 expression in prostatic intraepithelial neoplasia and human prostate cancer, Prostate 60 (4) (2004) 367–371, https://doi.org/10.1002/(ISSN)1097-004510.1002/pros.v60:410.1002/pros.20064.

[11] G.P. Carlson, Comparison of the effects of pyridine and its metabolites on rat liver and kidney, Toxicol. Lett. 85 (3) (1996) 173–178, https://doi.org/10.1016/0378-4274(96)03660-0.

[12] D.C. Pryde, D. Dalvie, Q. Hu, P. Jones, R.S. Obach, T.-D. Tran, Aldehyde Oxidase: An Enzyme of Emerging Importance in Drug Discovery, J. Med. Chem. 53 (24) (2010) 8441–8460, https://doi.org/10.1021/jm100888d.

[13] S.D. Martina, K.S. Vesta, T.L. Ripley, Etoricoxib: A Highly Selective COX-2 Inhibitor, Ann. Pharmacother. 39 (5) (2005) 854–862, https://doi.org/10.1345/aph.1E543.

[14] S. Tatar, S. Atmaca, Determination of amlodipine in human plasma by high-performance liquid chromatography with fluorescence detection, J. Chromatogr. B Biomed. Appl. 758 (2) (2001) 305–310, https://doi.org/10.1016/S0378-4347(01)00197-9.

[15] G. Papeo, H. Posteri, D. Borghi, A.A. Busel, F. Caprera, E. Casale, M. Ciomei, A. Cirla, E. Corti, M. D'Anello, M. Fasolini, B. Forte, A. Galvani, A. Isacchi, A. Khvat, M.Y. Krasavin, R. Lupi, P. Orsini, R. Perego, E. Pesenti, D. Pezzetta, S. Rainoldi, F. Riccardi-Sirtori, A. Scolaro, F. Sola, F. Zuccotto, E.R. Felder, D. Donati, A. Montagnoli, Discovery of 2-[1-(4,4-Difluorocyclohexyl)piperidin-4-yl]-6-fluoro-3-oxo-2,3-dihydro-1H-isoindole-4-carboxamide (NMS-P118): A Potent, Orally Available, and Highly Selective PARP-1 Inhibitor for Cancer Therapy, J. Med. Chem. 58 (17) (2015) 6875–6898, https://doi.org/10.1021/acs.jmedchem.5b00680.

[16] K. Bozorov, J.y. Zhao, L.F. Nie, H.-R. Ma, K. Bobakulov, R. Hu, N. Rustamova, G. Huang, T. Efferth, H.A. Aisa, Synthesis and in vitro biological evaluation of novel diaminothiophene scaffolds as antitumor and anti-influenza virus agents, Part 2, RSC Adv. 7 (50) (2017) 31417–31427, https://doi.org/10.1039/C7RA04808D.

[17] M.T. Burger, W. Han, J. Lan, G. Nishiguchi, C. Bellamacina, M. Lindval, G. Atallah, Y.u. Ding, M. Mathur, C. McBride, E.L. Beans, K. Muller, V. Tamez, Y. Zhang, K. Huh, P. Feucht, T. Zavorotinskaya, Y. Dai, J. Holash, J. Castillo, J. Langowski, Y. Wang, M.Y. Chen, P.D. Garcia, Structure Guided Optimization, in Vitro Activity, and in Vivo Activity of Pan-PIM Kinase Inhibitors, ACS Med. Chem. Lett. 4 (12) (2013) 1193–1197, https://doi.org/10.1021/ml400307j.

[18] P.D. Garcia, J.L. Langowski, Y. Wang, M. Chen, J. Castillo, C. Fanton, M. Ison, T. Zavorotinskaya, Y. Dai, J. Lu, X.-H. Niu, S. Basham, J. Chan, J. Yu, M. Doyle, P. Feucht, R. Warne, J. Narberes, T. Tsang, C. Fritsch, A. Kauffmann, E. Pfister, P. Drueckes, J. Trappe, C. Wilson, W. Han, J. Lan, G. Nishiguchi, M. Lindvall, C. Bellamacina, J.A. Aycinena, R. Zang, J. Holash, M.T. Burger, Pan-PIM Kinase Inhibition Provides a Novel Therapy for Treating Hematologic Cancers, Clin. Cancer Res. 20 (7) (2014) 1834–1845, https://doi.org/10.1158/1078-0432.CCR-13-2062.

[19] A.T.A. Boraei, H.K. Ashour, E.S.H. El Tamany, N. Abdelmoaty, A.I. El-Falouji, M. S. Gomaa, Design and synthesis of new phthalazine-based derivatives as potential EGFR inhibitors for the treatment of hepatocellular carcinoma, Bioorg. Chem. 85 (2019) 293–307, https://doi.org/10.1016/j.bioorg.2018.12.039.

[20] A.T.A. Boraei, M.S. Gomaa, E.S.H. El Ashry, A. Duerkop, Design, selective alkylation and X-ray crystal structure determination of dihydro-indolyl-1,2,4-triazole-3-thione and its 3-benzylsulfanyl analogue as potent anticancer agents, Eur. J. Med. Chem. 125 (2017) 360–371, https://doi.org/10.1016/j.ejmech.2016.09.046.

[21] A.T.A. Boraei, P.K. Singh, M. Sechi, S. Satta, Discovery of novel functionalized 1,2,4-triazoles as PARP-1 inhibitors in breast cancer: Design, synthesis and antitumor activity evaluation, Eur. J. Med. Chem. 182 (2019) 111621, https://doi.org/10.1016/j.ejmech.2019.111621.

[22] M.S. Nafie, A.M. Amer, A.K. Mohamed, E.S. Tantawy, Discovery of novel pyrazolo [3,4-b]pyridine scaffold-based derivatives as potential PIM-1 kinase inhibitors in breast cancer MCF-7 cells, Bioorg. Med. Chem. 28 (24) (2020) 115828, https://doi.org/10.1016/j.bmc.2020.115828.

[23] N.S. El-Gohary, S.S. Hawas, M.T. Gabr, M.I. Shaaban, M.B. El-Ashmawy, New series of fused pyrazolopyridines: Synthesis, molecular modeling, antimicrobial, antiquorum-sensing and antitumor activities, Bioorg. Chem. 92 (2019) 103109, https://doi.org/10.1016/j.bioorg.2019.103109.
[24] N.S. El-Gohary, M.I. Shaaban, New pyrazolopyridine analogs: Synthesis, antimicrobial, antiquorum-sensing and antitumor screening, Eur. J. Med. Chem. 152 (2018) 126–136, https://doi.org/10.1016/j.ejmech.2018.04.025.
[25] N.S. El-Gohary, M.I. Shaaban, Design, synthesis, antimicrobial, antiquorum-sensing and antitumor evaluation of new series of pyrazolopyridine derivatives, Eur. J. Med. Chem. 157 (2018) 729–742, https://doi.org/10.1016/j.ejmech.2018.08.008.
[26] M. Bachmann, H. Hennemann, P.X. Xing, I. Hoffmann, T. Möröy, The Oncogenic Serine/Threonine Kinase Pim-1 Phosphorylates and Inhibits the Activity of Cdc25C-associated Kinase 1 (C-TAK1) A NOVEL ROLE FOR Pim-1 AT THE G2/M CELL CYCLE CHECKPOINT, J. Biol. Chem. 279 (46) (2004) 48319–48328, https://doi.org/10.1074/jbc.M404440200.
[27] T.L.T. Aho, J. Sandholm, K.J. Peltola, H.P. Mankonen, M. Lilly, P.J. Koskinen, Pim-1 kinase promotes inactivation of the pro-apoptotic Bad protein by phosphorylating it on the Ser112 gatekeeper site, FEBS Lett. 571 (2004) 43–49, https://doi.org/10.1016/j.febslet.2004.06.050.
[28] M.S. Nafie, K. Arafa, N.K. Sedky, A.A. Alakhdar, R.K. Arafa, Triaryl dicationic DNA minor-groove binders with antioxidant activity display cytotoxicity and induce apoptosis in breast cancer, Chem.-Biol. Interact. 324 (2020) 109087, https://doi.org/10.1016/j.cbi.2020.109087.
[29] E.M. Gad, M.S. Nafie, E.H. Eltamany, M.S.A.G. Hammad, A. Barakat, A.T.A. Boraei, Discovery of New Apoptosis-Inducing Agents for Breast Cancer Based on Ethyl 2-Amino-4,5,6,7-Tetra Hydrobenzo[b]Thiophene-3-Carboxylate: Synthesis, In Vitro, and In Vivo Activity Evaluation, Molecules 25 (2020) 2523, https://doi.org/10.3390/molecules25112523.
[30] C.A. Lipinski, F. Lombardo, B.W. Dominy, P.J. Feeney, Experimental and computational approaches to estimate solubility and permeability in drug discovery and development settings1PII of original article: S0169-409X(96)00423-1. The article was originally published in Advanced Drug Delivery Reviews 23 (1997) 3–25.1, Adv. Drug Deliv. Rev. 46 (2001) 3–26, https://doi.org/10.1016/S0169-409X(00)00129-0.
[31] C.A. Lipinski, Lead- and drug-like compounds: the rule-of-five revolution, Drug Discov. Today: Technol. 1 (2004) 337–341, https://doi.org/10.1016/j.ddtec.2004.11.007.
[32] P.D. Leeson, B. Springthorpe, The influence of drug-like concepts on decision-making in medicinal chemistry, Nat. Rev. Drug Discov. 6 (2007) 881–890, https://doi.org/10.1038/nrd2445.
[33] D.E. Clark, S.D. Pickett, Computational methods for the prediction of 'drug-likeness', Drug Discov. Today 5 (2) (2000) 49–58, https://doi.org/10.1016/S1359-6446(99)01451-8.
[34] A.K. Ghose, T. Herbertz, R.L. Hudkins, B.D. Dorsey, J.P. Mallamo, Knowledge-Based, Central Nervous System (CNS) Lead Selection and Lead Optimization for CNS Drug Discovery, ACS Chem. Neurosci. 3 (1) (2012) 50–68, https://doi.org/10.1021/cn200100h.
[35] D.F. Veber, S.R. Johnson, H.-Y. Cheng, B.R. Smith, K.W. Ward, K.D. Kopple, Molecular properties that influence the oral bioavailability of drug candidates, J. Med. Chem. 45 (12) (2002) 2615–2623, https://doi.org/10.1021/jm020017n.
[36] R. Ian, Freshney, Culture of animal cells: a manual of basic technique and specialized applications, Wiley-Blackwell, Hoboken, N.J., 2010.
[37] T. Mosmann, Rapid colorimetric assay for cellular growth and survival: Application to proliferation and cytotoxicity assays, J. Immunol. Methods 65 (1-2) (1983) 55–63, https://doi.org/10.1016/0022-1759(83)90303-4.
[38] E.S. Tantawy, A.M. Amer, E.K. Mohamed, M.M. Abd Alla, M.S. Nafie, Synthesis, characterization of some pyrazine derivatives as anti-cancer agents: In vitro and in Silico approaches, J. Mol. Struct. 1210 (2020) 128013, https://doi.org/10.1016/j.molstruc.2020.128013.
[39] A.A.M. Sarhan, A.T.A. Boraei, A. Barakat, M.S. Nafie, Discovery of hydrazide-based pyridazino[4,5- *b*]indole scaffold as a new phosphoinositide 3-kinase (PI3K) inhibitor for breast cancer therapy, RSC Adv. 10 (33) (2020) 19534–19541, https://doi.org/10.1039/D0RA02798G.
[40] M.S. Nafie, S. Mahgoub, A.M. Amer, Antimicrobial and antiproliferative activities of novel synthesized 6-(quinolin-2-ylthio) pyridine derivatives with molecular docking study as multi-targeted JAK2/STAT3 inhibitors, Chem. Biol. Drug Des. 97 (3) (2021) 553–564, https://doi.org/10.1111/cbdd.v97.310.1111/cbdd.13791.
[41] S.W. Kattan, M.S. Nafie, G.A. Elmgeed, W. Alelwani, M. Badar, M.A. Tantawy, Molecular docking, anti-proliferative activity and induction of apoptosis in human liver cancer cells treated with androstane derivatives: Implication of PI3K/AKT/mTOR pathway, J. Steroid Biochem. Mol. Biol. 198 (2020) 105604, https://doi.org/10.1016/j.jsbmb.2020.105604.
[42] A.I. Khodair, M.A. Alsafi, M.S. Nafie, Synthesis, molecular modeling and anti-cancer evaluation of a series of quinazoline derivatives, Carbohydr. Res. 486 (2019) 107832, https://doi.org/10.1016/j.carres.2019.107832.
[43] M.S. Nafie, M.A. Tantawy, G.A. Elmgeed, Screening of different drug design tools to predict the mode of action of steroidal derivatives as anti-cancer agents, Steroids 152 (2019) 108485, https://doi.org/10.1016/j.steroids.2019.108485.
[44] E. Youssef, M.A. El-Moneim, W. Fathalla, M.S. Nafie, Design, synthesis and antiproliferative activity of new amine, amino acid and dipeptide-coupled benzamides as potential sigma-1 receptor, J. Iran. Chem. Soc. 17 (10) (2020) 2515–2532, https://doi.org/10.1007/s13738-020-01947-6.